

Anisotropic Rheology of Non-spherical Grains

by

Barbaros Ozyuksel

B.Sc., University of Turkish Aeronautical Association, 2017

A Report Submitted in Partial Fulfillment of the
Requirements for the Degree of

Master of Engineering

in the Department of Mechanical Engineering

© Barbaros Ozyuksel, 2021
University of Victoria

All rights reserved. This dissertation may not be reproduced in whole or in part, by photocopying or other means, without the permission of the author.

Anisotropic Rheology of Non-spherical Grains

by

Barbaros Ozyuksel

B.Sc., University of Turkish Aeronautical Association, 2017

Supervisory Committee

Dr. Ben Nadler, Supervisor
(Department of Mechanical Engineering)

Dr. Rustom B. Bhiladvala, Departmental Member
(Department of Mechanical Engineering)

ABSTRACT

The flow of granular materials is the subject of various academic research and industrial applications. The rheology of granular materials spans from packing, sorting and transportation of the pharmaceuticals to the study of avalanche dynamics. The rheology of shape isotropic (spherical) materials has been studied extensively and successful constitutive stress response models are present in the literature. In most real-life applications the grains are shape anisotropic (ellipsoidal), and their rheological and mechanical response is more complex than spherical grains. The shape anisotropy of the grains brings the effect of the grain orientation to their response. Isotropic granular rheology models neglect the effect of the grain orientation and shape on the mechanical response of the system. This report proposes a novel continuum stress response model based on isotropic granular rheology and utilizes a kinematic continuum model to capture the effect of the grain orientation. The representation theorem has been used to obtain the full description of the novel isotropic tensor valued function of the tensor variable. Dissipation inequality applied as a guide during the construction of the continuum model. The model predictions showed good agreement with the available experimental results of the simple shear flow at the steady-state. To reveal the complete capabilities of the model, the 2-D simple shear flow was studied. The results indicated that the model well captured the non-monotonic behaviour of the effective viscosity of the flow caused by the effect of grain shape and the orientation with two material parameters. This study revealed the future application potential of the proposed phenomenological model, and concluded as a successful step forward in understanding and modelling the complex character of the shape anisotropic granular materials.

Contents

Supervisory Committee	ii
Abstract	iii
Table of Contents	iv
List of Tables	vi
List of Figures	vii
Acknowledgements	viii
Dedication	ix
Nomenclature	x
1 Introduction	1
1.1 Rheology of Spherical Dense Granular Materials	2
1.2 Shape-Induced Anisotropy in Dense Granular Flow	4
2 Rheology of Anisotropic Granular Materials	11
2.1 The Kinematic Continuum Model to Predict the Orientation and Alignment of Non-spherical Grains	11
2.2 A Constitutive Rheology Law of Anisotropic Granular Materials . . .	14
2.2.1 Model Construction and Requirements	14
2.2.1.1 Isotropic function representation theorem	14
2.2.1.2 Dissipation Inequality	16
2.3 Comparison with Experimental Results and Material Parameter Determination	19
2.3.1 Tensorial Consistency	25

2.3.2	Dimensional Consistency	25
3	Shear Reversal Problem	26
3.1	Model Evolution to 2-D	28
3.2	Material Parameters for 2-D Problem	29
3.3	Governing Equations and the Procedure of Solving the Problem . . .	32
3.3.1	Governing Equations	32
3.3.1.1	Mass Balance	32
3.3.1.2	Linear Momentum Balance	33
3.3.1.3	Equations from Evolution of A	34
3.3.1.4	Initial Conditions	35
3.3.1.5	Boundary Conditions	36
3.3.1.6	Finite Difference Approximations	36
3.4	Results	37
3.4.1	Mechanical Response of the System	38
3.4.2	Orientation of the Grains	41
4	Conclusion	46
A	Additional Information	50
A.1	Governing Equations of the Reverse Direction	50
A.1.1	Linear Momentum Balance equations	50
A.1.2	Equations from the Evolution of Structure Tensor	50
	Bibliography	51

List of Tables

Table 3.1 Material Parameter Fit Results	31
Table 3.2 Material Parameters	31

List of Figures

Figure 1.1 Effective friction μ_s versus the shape ratio r_g [19]	6
Figure 1.2 Normal stress difference normalized by the pressure versus the shape ratio r_g [19]	7
Figure 1.3 Effective friction μ_s versus shape ratio r_g [25]	8
Figure 1.4 Effective friction μ_s versus the shape ratio r_g [20]	9
Figure 2.1 Stress component T_{12} versus the shape ratio r_g	21
Figure 2.2 Stress component T_{11} versus the shape ratio r_g	22
Figure 2.3 Stress component T_{33} versus the shape ratio r_g	23
Figure 2.4 Material parameters ϕ and η as a function of shape ratio r_g . .	24
Figure 3.1 Initial state of the problem	27
Figure 3.2 Steady-state of the problem when the orientation of the grains are no longer changing in time	27
Figure 3.3 Mesh and Initial Velocity Field Display	36
Figure 3.4 Velocity of the grains versus the relative position in the vertical axis of the flow where h is the flow height and y is the position in the flow height	38
Figure 3.5 Normalized shear stress at the walls versus dimensionless time $\hat{t} = t \dot{\gamma} $	39
Figure 3.6 Normalized shear stress with respect to A_{11}	40
Figure 3.7 Normalized shear stress with respect to A_{12}	41
Figure 3.8 A_{11} component of the structural tensor versus dimensionless time $\hat{t} = t \dot{\gamma} $	43
Figure 3.9 A_{22} component of the structural tensor versus dimensionless time $\hat{t} = t \dot{\gamma} $	44
Figure 3.10 A_{12} component of the structural tensor versus dimensionless time $\hat{t} = t \dot{\gamma} $	45

ACKNOWLEDGEMENTS

First of all, I would like to thank my graduate supervisor, **Dr. Ben Nadler**, for his endless support throughout this project. Without his guidance and patience, this project could not be completed. His door was always open whenever I needed help on whether on academic or personal matters. I am very lucky that I got the chance to know and research with him.

There were rough patches during the time of this study. I would like to express my special thanks to **Stephen Wade** for his help and support in those tough times. During my co-op work terms under his supervision, I found my future career path. His contribution is inestimable to my personal development and professional career.

The supreme guide in life is science.

Mustafa Kemal Ataturk

DEDICATED

To my significant other İrem Şıřmantürk
and my family Pınar, Sema and Behiç Özyüksel
without whom this study could not be completed.

NOMENCLATURE

L	Spatial gradient of the velocity vector
D	The rate of deformation tensor (symmetric part of L)
D^{dev}	Deviatoric part of the tensor D
 D 	The Euclidean norm of the rate of deformation tensor
W	Spin tensor (skew symmetric part of L)
A	Second order structure tensor of particle orientation
A^{dev}	Deviatoric part of the tensor A
$\dot{\mathbf{A}}$	Evolution of the tensor A (material time derivative)
R	The director tensor
r_g	The shape ratio of the grains
DEM	Discrete Element Method
Q	The aspect ratio of the grains

Chapter 1

Introduction

Granular materials and the flow of grains is a subject in various science fields and industrial applications. The study of granular rheology is a crucial research field in physics, geology and geophysics to study the stability of slopes, mechanics of soils, the flow of avalanches and mining and exploiting the earth's resources. On the other hand, the flow of the grains is ubiquitous when there are sorting, transporting or packing tasks in industrial applications. Most of the granular materials in real-life conditions are not spherical or well-shaped. Often, they are randomly shaped or packed such as rice, lentils, drugs, rocks and soil particles. In the literature, the rheology of the well-shaped dry stiff grains has been well studied experimentally and numerically. These studies are useful to reveal the rich research and application potential of the real-life problems with randomly shaped and oriented grains. Regardless of the shape of the granular materials, they can behave in three different ways. They behave like gases when they are under strong agitation, fluid-like under slow motions and like solids when there is no disturbance present.

Continuum models are required where full-scale physical experiments are not feasible due to the time, cost and resource limitations to study complex problems. Solid behaviour and gas behaviour of granular materials studied by soil mechanics and kinetic theory respectively, and phenomenological models have been proposed [11, 21]. In the case of fluid-like behaviour of granular flows, there were many attempts to formulate a constitutive model, but researchers could not come to an agreement [2, 17, 22]. In 2006, Jop et al. [15] proposed the well-known $\mu(I)$ rheology for dry dense granular flows.

1.1 Rheology of Spherical Dense Granular Materials

Fluid-like behaviour of granular materials attracted more scientists in the last fifteen years after a novel constitutive model presented by Jop et al. [15] for the well-shaped dry granular flows. Jop, Forterre and Pouliquen established a constitutive model for the internal stresses developed in the dense regime of incompressible granular flows. They managed to quantitatively capture the behaviour of the flows without any fit parameters according to their claim. The study acknowledges Da Cruz's [8] and Jordanoff's [14] as a framework where they showed that shear stress is proportional to the normal stress with the Savage number or Coulomb number using simple shear numerical simulations and experimental work [1, 23]. The Savage number or the inertial number according to [8] has the following form

$$I = \frac{\dot{\gamma}d}{\sqrt{P/\rho}}, \quad (1.1)$$

and the shear stress is defined as

$$\tau = \mu(I)P \quad (1.2)$$

where P denotes the isotropic pressure, ρ is the material density, d is the grain diameter and $\mu(I)$ is the friction coefficient. The friction coefficient $\mu(I)$ has the form

$$\mu(I) = \mu_s + \frac{\mu_2 - \mu_s}{I_0/I + 1} \quad (1.3)$$

where μ_s is the critical friction coefficient when inertial number I approaches to zero. The body acts as an elastic solid when $|\tau| < \mu_s P$. μ_2 is the limit value at high inertial number when the shear rate is very high, and I_0 is a material constant determined by experiments. Since the form (1.2) was not applicable when there is shear in different directions, Jop [15] proposed the well-known $\mu(I)$ rheology in the form

$$\mathbf{T} = -P\mathbf{I} + P\mu(I)\frac{\mathbf{D}}{\|\mathbf{D}\|}, \quad (1.4)$$

where inertial number (I) defined as

$$I = \frac{\|\mathbf{D}^{\text{dev}}\|d}{\sqrt{P/\rho}}. \quad (1.5)$$

The \mathbf{D} is the rate of deformation tensor which is the symmetric part of the velocity gradient, and $\|\mathbf{D}\|$ is the Euclidean norm of \mathbf{D} which calculated as $\|\mathbf{D}\| = \sqrt{\mathbf{D} \cdot \mathbf{D}} = \sqrt{\text{tr} \mathbf{D}^2}$.

The inertial number I , is the square root of the Savage number or the Coulomb number. It is a dimensionless measure of the ratio of deformation time scale to inertial time scale [15]. The purpose of the inertial number is to relate the deformation rate to the effective viscosity. $\mu(I)$ rheology has been shown to be successful in applications where time derivatives and spatial gradients of the velocity vector are not large.

$\mu(I)$ rheology is a capable tool to study the rheology of incompressible dry isotropic granular material flows. Numerical models have been build upon for different applications. Chauchat and Medale [6] is one example where they propose a new numerical model to use the $\mu(I)$ rheology to solve the steady-state dense granular flows. They compare their model with 3 different regularisation methods with $\mu(I)$ rheology relationships and validate the results using analytical solutions of the vertical-chute flow and the flow on an inclined plane. Also, they implemented their model to solve the flow on a heap and the chute flow over a cylinder.

$\mu(I)$ rheology is applicable where the shape of the grains can be fully defined by their diameter d . Therefore, the model is limited to spherical grains. However, as mentioned earlier the grains in nature and industrial applications are not always spherical. Non-spherical grains, such as prolate or oblate grains demonstrate a more complicated mechanical response compared to spherical grains. Their microscopic interaction is much more complex due to the fact that they can contact each other on an area unlike spherical which can only contact on a point. Also, ellipsoidal grains can jam or tangle each other easier compared to the spherical due to their more random and intricate contact network.

1.2 Shape-Induced Anisotropy in Dense Granular Flow

The richness of the ellipsoidal grain orientation and mechanical response has been the motivation of many numerical and experimental studies. These studies yielded interesting insights where scientists observed that grain shape strongly affects the alignment, orientation and mechanical response in the flow.

Azema et al. [3] investigated the rheological behaviour of the spherical and elongated particles with different degrees of homogeneities and mixture ratios under 2-D biaxial tests by contact dynamics method. They pointed out that the shear strength increases when the mixture has more elongated particles. Therefore their experiment reveals that it is harder to shear the elongated particles compared to spherical particles. Also, they explained the fact by stating that the elongated particles experience more friction than spherical particles and align themselves perpendicular to the major principal stress direction. In [27], Wegner et al. experimentally studied the effects of the grain shape on the packing and the dilatancy. They conducted an experiment with a split bottom container filled with various granular materials and measured rheological properties with X-ray tomography. Their experiment pointed out that the packing density in the shear zone is less for shape anisotropic particles compared to spherical particles. Also, they argue that there are two competing influences on the reduction of friction which are the reduction by dilatancy and the reduction by alignment. Azema and Radjai [4] numerically studied the mechanical response of the elongated granular material under the biaxial compression test. They showed that the solid fraction is following a non-monotonous behaviour with the particle elongation. It increases as the particle's elongation increases up to a certain value then decreases as the elongation of the grains further increases regardless of the shear strain. Later on, this finding was supported by Wegner et al. [27] with an experimental result. Cleary and Sawley [7] studied the effect of particle aspect ratio on the flow properties with the discrete element method (DEM). They pointed out that the increase in the aspect ratio of the grains leads up to a 29 percent decrease in the flow rate of the grains. Their finding supports Azema's claim where he pointed out that it is harder to shear the elongated particles compared to spherical [3]. Furthermore, Cleary and Sawley hold the position that elongated particles behave like deforming continua which is quite different than the free-flowing independent spherical particles. Börzönsyi et al. [5] conducted an experimental and numerical study on the orientational order and

alignment of elongated granular materials. They indicate that the average alignment angle, measured with respect to the shear flow direction, is independent of shear rate. They further assert that the average alignment angle decreases with increasing aspect ratio. This behaviour is explained by the hindering effect of the elongated grains. In other words, they point out that the elongated grains experience more alignment than the agitation effect due to collisions. As indicated by Börzönsyi the average alignment angle is independent of the shear rate. However, Farhadi and Behringer [10] observe that slowly sheared elliptical particles have stronger rate dependence than disk particles and they claim that the dependence is the outcome of the orientational degree of freedom. Furthermore, they advocate the view that anisotropic granular materials do not have orientational ordering property, but have a property that rotations due to collisions can change the density and stresses associated which is a contrary statement to many studies.

Shape anisotropic granular materials not only consist of well-shaped prolate or oblate grains. Irregularly shaped particles are very important in geotechnical and powder engineering. Moreover, in most of the real-life applications, the particles are irregularly shaped. The rheology of irregularly shaped granular materials attracted attention as the rheology of ellipsoidal grains did. However, the complicated characteristic of irregularly shaped particles and packing add another degree of complexity to the problems. Therefore, reproducing the results of experimental studies using DEM simulations is still the biggest challenge. In [16], Katagiri, Matsushima and Yamada studied the irregularly shaped particles with the direct element method (DEM). They modelled randomly shaped particles with 4 and 10- element models which generate a shape by unifying 4 or 10 spheres to approximate the shape of the realistic particles. They show that their particles which are generated by the 10-element model can capture the shear behaviour of relatively dense specimens under constant confining pressure simple shear test. Zhou and colleagues [28] studied the same topic but with a clump generation by the overlapping multi-sphere clump method (OMCM) in their direct element method simulations. Zhou et al. [28] state that randomly shaped particles increase the inter-particle interlocking, shear resistance and shear-induced dilation of the sands. Moreover, they note that realistic particles have more friction mobilization.

Nagy et al. [19] numerically studied frictionless elongated spherocylinders under the simple shear test and measured the rheological quantities as a function of inertial number (I) and grain shape. Their findings establish that μ_s , effective friction

coefficient, shows a non-monotonic behaviour with the increase in the elongation of grain shape. An intuitive parameter, the shape ratio r_g , has been presented in [18] to conveniently define the grain shape. The shape ratio defines as $r_g = l + d/l - d$, where l is the length and d is the diameter of the grains. The shape ratio is bounded as $-1 < r_g < 1$. It takes positive and increasing values as the elongation of the prolate grains increases, and negative and decreasing for oblate grains as their flatness increases. It is shown in figure 1.1 by (Nagy et al., 2017, p.4) that for spherocylinders the effective friction coefficient steeply increases with increased shape ratio up to $r_g = 0.024$ then decreases with the further increase in the shape ratio.

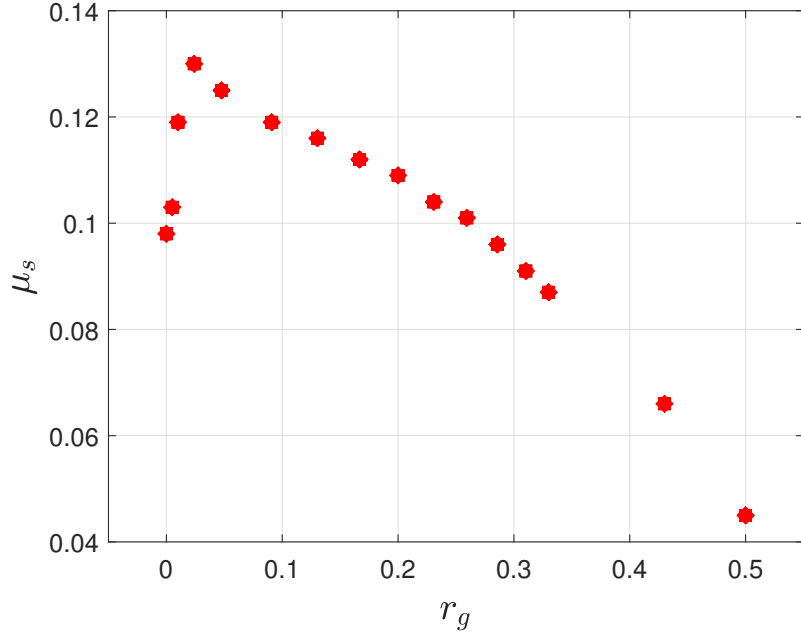


Figure 1.1: Effective friction μ_s versus the shape ratio r_g [19]

Note. From Nagy, Dániel B., Philippe Claudin, Tamás Börzsönyi, et al. 'Rheology of Dense Granular Flows for Elongated Particles', *Physical Review E*, vol. 96/no. 6-1, (2017), pp. 062903-062903. 2017 American Physical Society.

In [19] Nagy et al. used the empirical form

$$\mu(I) \approx \mu_s + \mu_1 I^\alpha \quad (1.6)$$

instead of (1.3) as originally proposed in [15]. They used the empirical form and took α as 0.4 to extrapolate the μ_s where inertial number is approaching zero. A similar non-monotonic characteristic has been observed in figure 1.2 from (Nagy et al., 2017,

p.4) for the normal stress differences. The normal stress difference increases with the increase in shape ratio up to $r_g = 0.43$ then decreases with the further increase in the shape ratio of the grains.

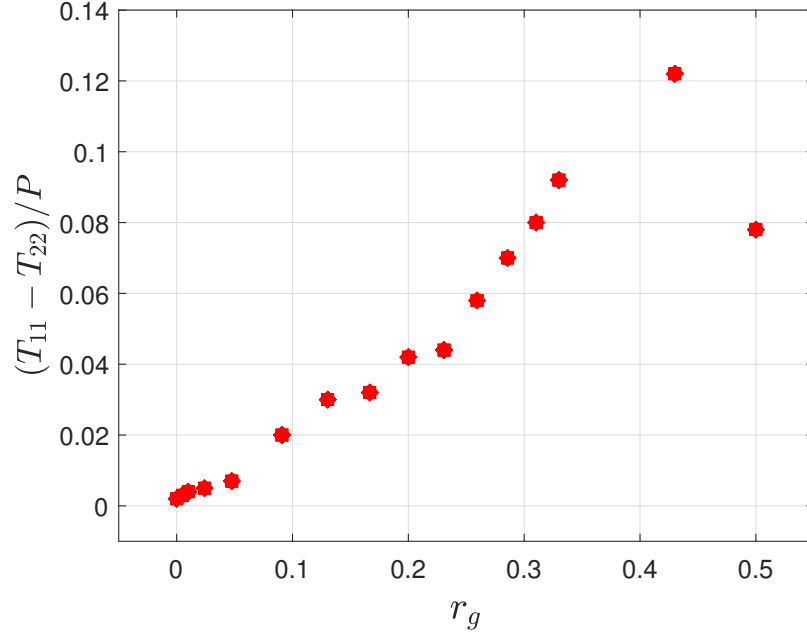


Figure 1.2: Normal stress difference normalized by the pressure versus the shape ratio r_g [19]

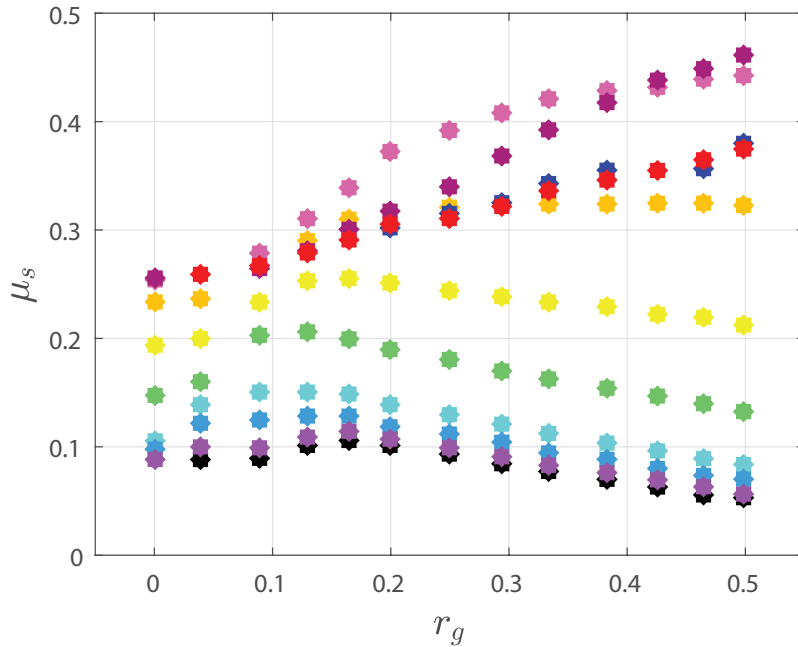
Note. From Nagy, Dániel B., Philippe Claudin, Tamás Börzsönyi, et al. 'Rheology of Dense Granular Flows for Elongated Particles', *Physical Review E*, vol. 96/no. 6-1, (2017), pp. 062903-062903. 2017 American Physical Society.

Later on, these findings were supported by Somfai et al. [24], they also reported a non-monotonic behaviour of the effective friction with the increase in shape ratio. In 2018, Trulsson [25] studied both frictionless and frictional particles in 2-D simple shear in order to study the effect of interparticle friction on rheological properties of the flow. Unlike Nagy, Trulsson used the following empirical form to quantify the $\mu(I)$.

$$\mu(I) = \mu_s + \frac{c_\mu}{1 + (I_0/I)^{\beta^\mu}} \quad (1.7)$$

where c_μ , I_0 and β^μ are the material parameters, such as shape, interparticle friction coefficient and polydispersity which are related to the assembly of grains. Similar to [19], [25] also reported a non-monotonic behaviour of effective friction coefficient with the increased shape ratio for the grains with 0.1 or lower interparticle friction coefficient in figure 1.3 from (Trulsson, 2018, p.728). However, particles with an in-

terparticle friction coefficient of 0.4 or higher showed a monotonic increase in effective friction with an increased shape ratio.



Interparticle Friction Coefficient			
● $\mu_p = 0$	● $\mu_p = 0.01$	● $\mu_p = 0.2$	● $\mu_p = 4$
● $\mu_p = 0.001$	● $\mu_p = 0.04$	● $\mu_p = 0.4$	● $\mu_p = 10$
● $\mu_p = 0.004$	● $\mu_p = 0.1$	● $\mu_p = 1$	

Figure 1.3: Effective friction μ_s versus shape ratio r_g [25]

Note. From Trulsson, Martin. 'Rheology and Shear Jamming of Frictional Ellipses', Journal of Fluid Mechanics, vol. 849/(2018), pp. 718-740. Cambridge University Press 2018.

Although Trulsson [25] conducted DEM simulations with an interparticle friction coefficient, μ_p , above 0.4, he also claims that these conditions are not realistic, and $\mu_p = 4$ is the finite friction limit. Findings of [19] and [25] agree with Guises et al. [12] where they have also reported a non-monotonic behaviour. In 2020, Nagy et al. [20] conducted the same 3-D DEM simulations as in their previous work [19], but with the addition of the interparticle friction between the grains. They reported the same characteristic in figure 1.4 as Trulsson's [25] 2-D simulations where the only difference between the two studies is the addition of the third dimension.

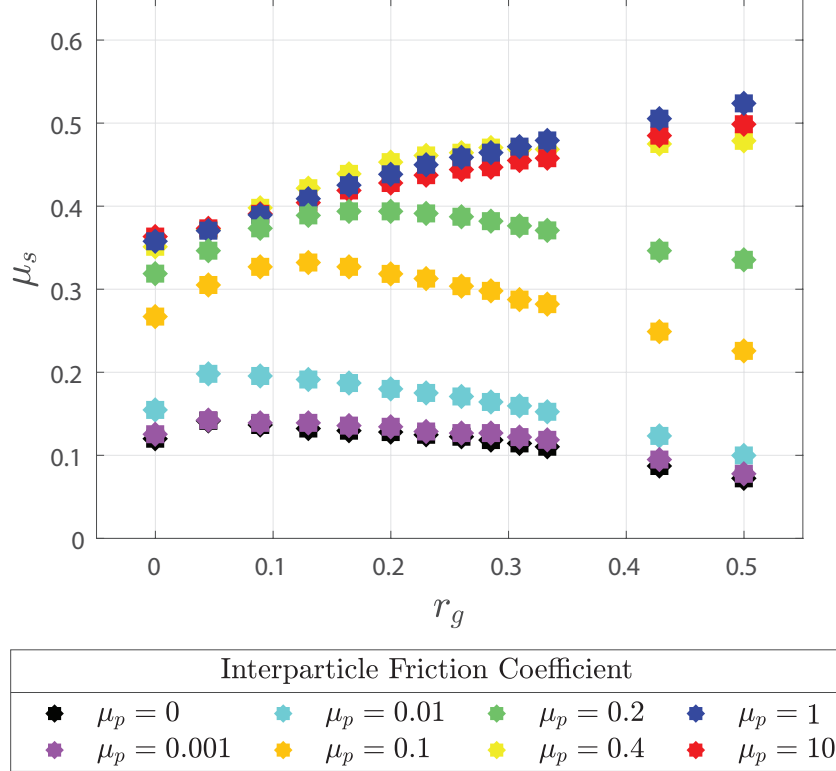


Figure 1.4: Effective friction μ_s versus the shape ratio r_g [20]

Note. From Nagy, Dániel B., Philippe Claudin, Tamás Börzsönyi, et al. 'Flow and Rheology of Frictional Elongated Grains', *New Journal of Physics*, vol. 22/no. 7, (2020), pp. 73008. Open Access.

It has been observed in the aforementioned studies that the collective motion of elongated grains yield to an orientation along the streamlines of the flow with an angle. The observation suggests that there is a powerful interconnection between the flow and particle orientation which affects the rheological response as well as the mechanical behaviour. This alignment behaviour along the streamlines is decreasing the effective friction of the system. Therefore, aligned elongated grains experience less shear resistance compared to grains that are in random and non-ordered state. It is clear that elongated grains' tenancy to align themselves along the streamlines yields to a non-monotonic behaviour in effective friction in low inertial number steady-state shear flow. It has been observed that the orientation and alignment of the grains also demonstrates non-monotonic behaviour as the grains get more and more elongated.

There are no available phenomenological constitutive model which can be used to predict the mechanical response of the ellipsoidal grains flow. An attempt has been made by Hidalgo et al. [13] by introducing a correction factor to the grain diameter d

and inertial number I . The effective particle size which they named it as d_{eff} is the projection of the grain length onto the perpendicular axis to the flow axis. The use of the new effective particle size in form (1.1) defines their effective inertial number

$$I_{eff} = \frac{\dot{\gamma}d_{eff}}{\sqrt{P/\rho}}. \quad (1.8)$$

The classical $\mu(I)$ rheology with this modified inertial term is not capable of predicting a non-monotonic behaviour. The behaviour is interpreted as the outcome of two competing factors which are the decrease in shear resistance by the ellipsoidal grain alignment and increased interlocking characteristic of ellipsoidal grains which increases the shear resistance. The form

$$\mu(I) = \mu_s + (\mu_2 - \mu_s)\frac{I}{I + I_0}, \quad (1.9)$$

from [13] only consists of one parameter, corrected $\mu(I)$, which tries to capture both increase and decrease in shear resistance as the orientation of the grains changes in time when undergoing deformation.

It is evident that the alignment of the grains and shape have a great effect on the mechanical response of elongated grains. There is no available model that can predict the mechanical response of the grains as the orientation in the flow changes over time. The main aim of this study is to propose a complete novel phenomenological constitutive model based on the well-received $\mu(I)$ rheology to predict the mechanical response of elongated grains which can capture the change in response due to change in orientation in time and the interlocking behaviour change due to the particle shape.

Chapter 2

Rheology of Anisotropic Granular Materials

2.1 The Kinematic Continuum Model to Predict the Orientation and Alignment of Non-spherical Grains

As discussed earlier, the initial orientation of the grains and the change in orientation over time have a great effect on the mechanical response of the grains. To predict the change in the orientation of the grains as they undergo deformation, a kinematic continuum model is needed. Nadler, Guillard and Einav [18] proposed a kinematic continuum model to predict the orientation of the grains using the spatial velocity gradient tensor \mathbf{L} and two material parameters which are the function of the grain shape. They use a second order structure tensor which they refer to as the structural tensor \mathbf{A} to uniquely determine the orientation state of the grains. Nadler et al. define the individual grain and its orientation by using its length, diameter and a unit vector that lies along the symmetry axis of the grain which is labeled as \mathbf{k} . By using a probability density function, f , it is postulated that

$$f(\mathbf{k}) \equiv f(-\mathbf{k}) \geq 0; \quad (2.1)$$

and the surface integral of the probability density function in 3-D Euclidean space over the unit sphere S^2 is

$$\oint_{S^2} f(\mathbf{k}) da = 1. \quad (2.2)$$

Using a 2nd order structure tensor they constructed the positive semi-definite symmetric tensor \mathbf{A} in the following form [18]

$$\mathbf{A} = \oint_{S^2} f(\mathbf{k}) \mathbf{k} \otimes \mathbf{k} da. \quad (2.3)$$

The symmetry property of \mathbf{A} is important to establish since it is planned to be included while constructing a constitutive law using the symmetric Cauchy stress tensor. The symmetry can be shown by taking the transpose of the definition of \mathbf{A} . The tensor product satisfies linearity properties which means $(\mathbf{y} \otimes \mathbf{w})^T = \mathbf{w} \otimes \mathbf{y}$. In this case, both sides of the tensor product are \mathbf{k} , therefore transposition does not change the basis. Hence,

$$\left(\oint_{S^2} f(\mathbf{k}) \mathbf{k} \otimes \mathbf{k} da \right)^T = \oint_{S^2} f(\mathbf{k}) \mathbf{k} \otimes \mathbf{k} da. \quad (2.4)$$

Nadler et al. [18] used the spectral representation of the symmetric \mathbf{A} , and established that

$$\mathbf{A} = \sum_{j=1}^3 a_j \mathbf{a}_j \otimes \mathbf{a}_j, \quad (2.5)$$

where a_1, a_2, a_3 are the positive eigenvalues. The associated orthogonal eigenvectors are $\mathbf{a}_1, \mathbf{a}_2, \mathbf{a}_3$ in E^3 Euclidean vector space. The summation of the eigenvalues is $\sum_{j=1}^3 a_j = 1$ since the $\text{tr } \mathbf{A} = 1$ which is guaranteed by $\oint_{S^2} f(\mathbf{k}) da = 1$. It is also important to show that \mathbf{A} is a positive semi-definite tensor since the property will be used when applying the dissipation inequality to the proposed model. It can be established by taking the dot product of any non-zero vector with \mathbf{A} operating on the same vector and showing that $\mathbf{m} \cdot \left(\oint_{S^2} f(\mathbf{k}) \mathbf{k} \otimes \mathbf{k} da \right) \mathbf{m} \geq 0$. The arbitrary non-zero vector \mathbf{m} can be taken inside of the surface integral since it is not a function of da . Then, one can use the definition of the tensor product, $(\mathbf{a} \otimes \mathbf{b}) \cdot \mathbf{c} = (\mathbf{b} \cdot \mathbf{c}) \mathbf{a}$, to establish that

$$\mathbf{m} \cdot \left(\oint_{S^2} f(\mathbf{k}) \mathbf{k} \otimes \mathbf{k} da \right) \mathbf{m} = \oint_{S^2} f(\mathbf{k}) (\mathbf{k} \cdot \mathbf{m})^2 da. \quad (2.6)$$

The term $f(\mathbf{k}) \equiv f(-\mathbf{k}) \geq 0$ always positive by definition, and $(\mathbf{k} \cdot \mathbf{m})^2$ is guaranteed to be greater than or equal to zero at all times. Hence, we can claim that \mathbf{A} is a positive semi-definite tensor. To find the evolution law of \mathbf{A} , the material time derivative is taken as

$$\dot{\mathbf{A}} = \frac{d}{dt} \oint_{S^2} f \mathbf{k} \otimes \mathbf{k} da = \oint_{S^2} f(\dot{\mathbf{k}} \otimes \mathbf{k} + \mathbf{k} \otimes \dot{\mathbf{k}}) da, \quad (2.7)$$

where $\dot{\mathbf{k}}$ is defined for a line element travelling in the flow as

$$\dot{\mathbf{k}} = \mathbf{W}\mathbf{k} + \lambda(\mathbf{D} - (\mathbf{k} \cdot \mathbf{D}\mathbf{k}))\mathbf{k}. \quad (2.8)$$

Then the evolution law with two material parameters presented in [18] as

$$\dot{\mathbf{A}} = \mathbf{W}\mathbf{A} - \mathbf{A}\mathbf{W} + \lambda(\mathbf{D}\mathbf{A} + \mathbf{A}\mathbf{D} - 2(\mathbf{A} \cdot \mathbf{D})\mathbf{A}) - \psi\|\mathbf{D}\|(\mathbf{A} - \mathbf{I}/3), \quad (2.9)$$

where \mathbf{W} is the spin tensor which is the skew symmetric part of the spatial velocity gradient defined as $\mathbf{W} = \frac{1}{2}(\mathbf{L} - \mathbf{L}^T)$, and \mathbf{D} is the rate of deformation tensor defined as the symmetric part of the spatial velocity gradient $\mathbf{D} = \frac{1}{2}(\mathbf{L} + \mathbf{L}^T)$. ψ and λ are two material parameters which are function of the shape ratio r_g . Nadler et al. [18] define the shape ratio of the grains as

$$r_g = \frac{\text{lenght} - \text{diameter}}{\text{lenght} + \text{diameter}}. \quad (2.10)$$

For prolate grains r_g takes a value in between 0 and 1, and for oblate grains it is in between -1 and 0.

Material parameter ψ is interpreted as the measure of misalignment due to particle contacts and shape during the flow hence it is expected to be a positive value since the tendency is assumed to be toward random distribution. Also, ψ is expected to be decreasing with the increase in the particles elongation since it is harder to rotate more elongated particles hence the rotation due to collision effect should be less effective. λ on the other hand is interpreted as the measure of the orientation convection, in other words it governs the alignment tendency of the grains with the rate of deformation. Nadler et al. [18] suggest that λ takes a value in between -1 and 1 according to the particle shape, and to be 0 for the spherical particles since the rotation due to collision does not change the orientation of the spherical particles. The model has been validated with direct elemental method (DEM) simple shear

simulations, which showed a good agreement with the simulation results. Based on DEM simulations, two empirical relationships have been presented in [18] for grains with the interparticle friction coefficient of 0.5 in the following forms for two material parameters

$$\lambda = \frac{2}{\phi} \tan^{-1}(5.5r_g), \quad (2.11)$$

$$\psi = 0.85 \exp(-4r_g^2). \quad (2.12)$$

The kinematic continuum model shows that it is well capturing the orientation of the elongated granular materials. Hence the model decided to be used as a foundation along with the $\mu(I)$ rheology to propose a stress response model for the anisotropic granular material.

2.2 A Constitutive Rheology Law of Anisotropic Granular Materials

2.2.1 Model Construction and Requirements

As discussed earlier, the main aim of this study is to propose a phenomenological stress response model that can capture the effect of particle orientation and shape that can be applied to various ellipsoidal grains. Hence, the model should be a function of the orientation tensor \mathbf{A} and the shape ratio r_g along with the other dependencies. The spherical $\mu(I)$ rheology's structure is

$$\mathbf{T} = \hat{\mathbf{T}}(I, P, \mathbf{D}). \quad (2.13)$$

Based on the (2.13) with the addition of the particle orientation and shape ratio the following structure is expected to capture the shape induced anisotropy in the mechanical response.

$$\mathbf{T} = \hat{\mathbf{T}}(I, P, \mathbf{D}, \mathbf{A}; r_g) \quad (2.14)$$

2.2.1.1 Isotropic function representation theorem

In order to use the representation theorem for isotropic tensor-valued functions of a tensor variable, the function must be isotropic. For a tensor function of a tensor variable to be named as isotropic it must satisfy the following for all orthogonal

tensors \mathbf{Q} .

$$\hat{\mathbf{T}}(I, P, \mathbf{QDQ}^T, \mathbf{QAQ}^T; r_g) = \mathbf{Q}\hat{\mathbf{T}}(I, P, \mathbf{D}, \mathbf{A}; r_g)\mathbf{Q}^T \quad (2.15)$$

In order the (2.15) to hold for all improper orthogonal tensors \mathbf{Q} , the \mathbf{D} and \mathbf{A} must be objective tensors, and effective viscosity $\mu(I)$ and shape ratio r_g must be objective scalars under superposed rigid body motion. The spatial tensors $\mathbf{D}^+ = \mathbf{QDQ}^T$ and $\mathbf{A}^+ = \mathbf{QAQ}^T$ transform objectively. Also, the scalars $I^+ = I$, $r_g^+ = r_g$ and $P^+ = P$ transform objectively under the superposed rigid body motion. Therefore, the tensor $\mathbf{T} = \hat{\mathbf{T}}(I, P, \mathbf{D}, \mathbf{A}; r_g)$ is proven to be an objective isotropic function.

Adopting the structure of the $\mu(I)$ rheology leads to splitting the spherical part and deviatoric part of stresses as

$$\mathbf{T} = -PI\mathbf{I} + \boldsymbol{\tau}, \quad (2.16)$$

where $\boldsymbol{\tau}$ is the function of \mathbf{D} , \mathbf{A} , I , P and r_g . Since \mathbf{T} is isotropic, $\boldsymbol{\tau}$ is guaranteed to be isotropic as well.

According to the representation theorem for isotropic tensor-valued functions of a 2nd order tensor, any isotropic function can be represented as

$$\boldsymbol{\tau}(\mathbf{N}) = \alpha_0\mathbf{I} + \alpha_1\mathbf{N} + \alpha_2\mathbf{N}^2, \quad (2.17)$$

where $\alpha_0, \alpha_1, \alpha_2$ are the scalar valued functions of the three invariants of \mathbf{N} [26]. In this study we propose that Cauchy stress tensor depends on \mathbf{D} , \mathbf{A} , P , I and r_g .

By using the isotropic function representation theorem the $\boldsymbol{\tau}$ can be represented as

$$\begin{aligned} \boldsymbol{\tau}(I, P, \mathbf{D}, \mathbf{A}; r_g) = & \alpha_0\mathbf{I} + \alpha_1\mathbf{D} + \alpha_2\mathbf{D}^2 + \alpha_3\mathbf{A} + \alpha_4\mathbf{A}^2 + \alpha_5(\mathbf{AD} + \mathbf{DA}) \\ & + \alpha_6(\mathbf{D}^2\mathbf{A} + \mathbf{AD}^2) + \alpha_7(\mathbf{DA}^2 + \mathbf{A}^2\mathbf{D}) + \alpha_8(\mathbf{D}^2\mathbf{A}^2 + \mathbf{A}^2\mathbf{D}^2). \end{aligned} \quad (2.18)$$

The Cayley-Hamilton theorem allows any positive integer power of any tensor \mathbf{T} to be expressed as the function of spatial identity tensor \mathbf{I} , \mathbf{T} and \mathbf{T}^2 since every tensor satisfies its own characteristic equation. For example, \mathbf{T}^3 can be represented by the help of its characteristic equation as

$$\mathbf{T}^3 - I_1(\mathbf{T})\mathbf{T}^2 + I_2(\mathbf{T})\mathbf{T} + I_3(\mathbf{T})\mathbf{I} = 0. \quad (2.19)$$

Therefore, the isotropic representation of $\boldsymbol{\tau}$ does not contain or need any cubic terms in \mathbf{A} and \mathbf{D} . $\alpha_p[I, P, I_0, I_1, I_2, I_3, I_4, I_5, I_6, I_7, I_8, I_9; r_g]$ are scalar valued functions of

the all linearly independent invariants of \mathbf{A} and \mathbf{D} . To be more specific the invariants are written as follows.

$$I_0 = \text{tr } \mathbf{D}, I_1 = \text{tr } \mathbf{D}^2, I_2 = \text{tr } \mathbf{D}^3, I_3 = \text{tr } \mathbf{A}, I_4 = \text{tr } \mathbf{A}^2, I_5 = \text{tr } \mathbf{A}^3, I_6 = \text{tr } \mathbf{D}\mathbf{A},$$

$$I_7 = \text{tr } \mathbf{D}^2\mathbf{A}, I_8 = \text{tr } \mathbf{D}\mathbf{A}^2, I_9 = \text{tr } \mathbf{D}^2\mathbf{A}^2.$$

One might further simplify the invariants and argue that since $\text{tr } \mathbf{D} = \text{div } \mathbf{v} = 0$ due to incompressibility, $\text{tr } \mathbf{A} = 1$ by definition of the tensor \mathbf{A} , and $\text{tr } \mathbf{D}^2 = \|\mathbf{D}\|^2$ which is included in the inertia number, (I), there are only 7 invariants.

The model construction started with using only the linear terms in \mathbf{A} . The idea was to start with the simplest form to propose a concise model that can be applied uncomplicatedly, and bring the quadratic terms if the model cannot capture the shape induced anisotropy. By only using the linear terms of \mathbf{A} from the equation (2.18), the model has the form

$$\mathbf{T} = -P\mathbf{I} + P\mu(I)\phi(r_g)[\bar{\mathbf{D}} + \eta(r_g)(\bar{\mathbf{D}}\mathbf{A} + \mathbf{A}\bar{\mathbf{D}} - 2/3(\bar{\mathbf{D}} \cdot \mathbf{A})\mathbf{I}) + \|\mathbf{D}\|\nu(r_g)\mathbf{A}^{\text{dev}}], \quad (2.20)$$

where $\bar{\mathbf{D}} = \mathbf{D}/\|\mathbf{D}\|$. ϕ, η and ν are the three unique material parameters which are the function of the shape ratio r_g , and $\mathbf{A}^{\text{dev}} = \mathbf{A} - \mathbf{I}/3$ is the spherical part of the tensor \mathbf{A} . One point out that the form (2.20) does not contain all the linear terms of the tensor \mathbf{A} since $\mathbf{D}^2\mathbf{A}$ is not included. The initial idea was to only use the linear terms in both \mathbf{A} and \mathbf{D} , however, the use of $\|\mathbf{D}\|$ term made the model non-linear in \mathbf{D} . The reason of including the term $\|\mathbf{D}\|$ in front of the $\nu(r_g)\mathbf{A}^{\text{dev}}$ was to make sure there are no stresses generated when there is no flow, and stresses $\mathbf{T} = -P\mathbf{I}$. Although the form (2.20) is non-linear in \mathbf{D} here we still do not include the quadratic terms of \mathbf{D} implicitly in the model for the sake of simplicity.

2.2.1.2 Dissipation Inequality

In the pure mechanical theory, when in the absence of stored elastic energy, but viscous dissipation of energy in the system, the dissipation inequality asserts that

$$\mathbf{T} \cdot \mathbf{D} \geq 0. \quad (2.21)$$

Applying this condition to the form (2.20), and rearranging $\|\mathbf{D}\|$ as the common multiplier gives the following condition

$$-P\mathbf{I} + \frac{P\mu(I)\phi(r_g)}{\|\mathbf{D}\|}[\mathbf{D} + \eta(r_g)(\mathbf{D}\mathbf{A} + \mathbf{A}\mathbf{D} - 2/3(\mathbf{D} \cdot \mathbf{A})\mathbf{I}) + \|\mathbf{D}\|^2\nu(r_g)\mathbf{A}^{\text{dev}}] \cdot \mathbf{D} \geq 0, \quad (2.22)$$

for all tensor \mathbf{D} and \mathbf{A} at all times. The distribution of the dot product to the form (2.22) yields to

$$\frac{P\mu(I)\phi}{\|\mathbf{D}\|}(\text{tr } \mathbf{D}^2 + 2\eta(\mathbf{D}^2 \cdot \mathbf{A}) + \|\mathbf{D}\|^2\nu\mathbf{A}^{\text{dev}} \cdot \mathbf{D}) \geq 0. \quad (2.23)$$

Note that $\mathbf{I} \cdot \mathbf{D} = 0$ due to incompressibility. Further simplifications can be done by using $\text{tr } \mathbf{D}^2 = \mathbf{I} \cdot \mathbf{D}^2 = \|\mathbf{D}\|^2$ equations as

$$\frac{P\mu(I)\phi}{\|\mathbf{D}\|}(\mathbf{I} \cdot \mathbf{D}^2 + 2\eta(\mathbf{D}^2 \cdot \mathbf{A}) + \nu(\mathbf{A}^{\text{dev}} \cdot \mathbf{D})\mathbf{I} \cdot \mathbf{D}^2) \geq 0. \quad (2.24)$$

Taking \mathbf{D}^2 as the common dot product outside the parenthesis brings the form 2.24 into

$$\frac{P\mu(I)\phi}{\|\mathbf{D}\|}[(1 + \nu(\mathbf{A}^{\text{dev}} \cdot \mathbf{D}))\mathbf{I} + 2\eta\mathbf{A}] \cdot \mathbf{D}^2 \geq 0. \quad (2.25)$$

$P, \mu(I)$ and $\|\mathbf{D}\|$ are positive at all times, therefore ϕ must be ≥ 0 to guarantee the requirement. Also, since \mathbf{D}^2 is a positive semi-definite tensor, the expression in the parenthesis must be a positive semi-definite tensor for the dot product to be positive at all times. Hence, the dissipation inequality set the condition that

$$\mathbf{z}^T[\mathbf{I} + 2\eta\mathbf{A} + \nu(\mathbf{A}^{\text{dev}} \cdot \mathbf{D})\mathbf{I}]\mathbf{z} > 0, \quad (2.26)$$

for every non-zero column vector \mathbf{z} . There is no guarantee that the term $\nu(\mathbf{A}^{\text{dev}} \cdot \mathbf{D})$ is positive at all times since \mathbf{A} and \mathbf{D} are independent from each other. Although there is a phenomenological model that relates \mathbf{A} to \mathbf{D} , still there is no guarantee that the dot product of each is going to be positive at all times. Hence, the material parameter ν is taken to be equal to 0 in order to avoid violating the dissipation inequality. Elimination of the material parameter ν leads to the restriction

$$\mathbf{z}^T[\mathbf{I} + (2\eta\mathbf{A})\mathbf{I}]\mathbf{z} > 0. \quad (2.27)$$

In order for tensor to be a positive semi-definite, it must be symmetric and all it's eigenvalues to be non-negative. The symmetry property is satisfied since \mathbf{A} and spatial identity tensor \mathbf{I} are symmetric, hence the addition of those two is also symmetric. The eigenvalue of the identity tensor is 1, and any non-zero vector is it's eigenvector. One can use the spectral representation of \mathbf{A} to bring the tensor in the equation 2.27 into the form

$$\mathbf{I} + 2\eta \sum_{j=1}^3 a_j \mathbf{a}_j \otimes \mathbf{a}_j,$$

and the eigenvalues of the tensor are

$$t_j = 1 + 2\eta a_j. \quad (2.28)$$

The biggest eigenvalue of the tensor \mathbf{A} , a_1 , is 0.3 when the orientation of the grains are isotropic and 1 when they are fully aligned. Therefore it is bounded as $1/3 \leq a_1 \leq 1$. η can take the smallest value when it is guaranteed that for all a_j the expression is greater than or equal to 0. The restriction $\eta \geq 1/2a_j$ is always satisfied when $\eta \geq -0.5$ since the biggest eigenvalue of the tensor \mathbf{A} is in the range $[1/3, 1]$. Hence, $\eta \geq -0.5$ is the requirement derived from the dissipation inequality. As a summary the restrictions and alterations that dissipation inequality posed are

$$\eta(r_g) \geq -0.5,$$

$$\phi(r_g) \geq 0,$$

$$\nu = 0.$$

Hence the initial proposed equation (2.20) reduces to

$$\mathbf{T} = -P\mathbf{I} + P\mu(I)\phi(r_g)(\bar{\mathbf{D}} + \eta(r_g)(\bar{\mathbf{D}}\mathbf{A} + \mathbf{A}\bar{\mathbf{D}} - 2/3(\bar{\mathbf{D}} \cdot \mathbf{A})\mathbf{I})). \quad (2.29)$$

The material parameter ϕ interpreted as it governs the tangling and interlocking characteristic of the elongated grains where more elongated grains, where shape ratio r_g approaching to 1 or -1, experience more interlocking effect due to extra grain to grain contact points. Therefore, ϕ is expected to be positive and monotonically increasing as the absolute value of the grains' shape ratio approaches ± 1 . On the other hand, η is interpreted as it governs the alignment characteristic of the grains as they undergo deformation. As the grains become more aligned the shear resistance

should decrease. Therefore, η is expected to be negative and monotonically decreasing as the absolute value of the grains' shape ratio approaches 1, but expected to be no less than -0.5.

2.3 Comparison with Experimental Results and Material Parameter Determination

The phenomenological equation (2.29) shaped with the help of isotropic function representation theorem and the dissipation inequality. A comparison with the available experimental data is needed to validate that the model is predicting and capturing the shape induced anisotropy of the granular flow. Nagy's [19] 3-D simple shear DEM simulations with frictionless spherocylinders found to be the most suitable experimental data set to test the model and determine the material parameters since they conduct simulations for different grain shape ratios including spherical, and cover low inertial number simple shear case as well as high inertial number faster flows. Since the focus of the constitutive model is to capture the non-monotonous behaviour of the critical friction coefficient, the model parameters need to be determined using experimental results where the inertial number is approaching to 0. λ and ψ determined for each shape ratio r_g using empirical relations (2.11) and (2.12) from [18]. Since the problem is steady-state, the time dependency $\frac{\partial \mathbf{A}}{\partial t} = 0$. Also, $(\text{grad } \mathbf{A})\mathbf{v} = 0$ because there is no gradient term in the kinematic model. Hence the left hand side of the equation (2.9) boils down to zero vector. Then the orientation tensor \mathbf{A} determined for the each case using the expression

$$\mathbf{0} = \mathbf{W}\mathbf{A} - \mathbf{A}\mathbf{W} + \lambda(\mathbf{D}\mathbf{A} + \mathbf{A}\mathbf{D} - 2(\mathbf{A} : \mathbf{D})\mathbf{A}) - \psi\|\mathbf{D}\|(\mathbf{A} - \mathbf{I}/2) \quad (2.30)$$

by substituting proper material parameters, and taking \mathbf{A} and \mathbf{D} as

$$\mathbf{D} = \frac{\dot{\gamma}}{2} \frac{\partial v_1}{\partial x_2} (\mathbf{e}_1 \otimes \mathbf{e}_2 + \mathbf{e}_2 \otimes \mathbf{e}_1),$$

$$\mathbf{W} = \frac{\dot{\gamma}}{2} \frac{\partial v_1}{\partial x_2} (\mathbf{e}_1 \otimes \mathbf{e}_2 - \mathbf{e}_2 \otimes \mathbf{e}_1).$$

In order to determine the material parameters ϕ and η , experimental stress results are needed to equate them to the phenomenological model. Components of the Cauchy stress tensor extracted from Nagy [19] where they reported the μ and normalized

normal stresses in the following forms

$$\mu = \frac{T_{12}}{T_{22}}, \quad (2.31)$$

$$\frac{N_1}{T_{22}} = \frac{T_{12} - T_{22}}{T_{22}}, \quad (2.32)$$

$$\frac{N_2}{T_{22}} = \frac{T_{22} - T_{33}}{T_{22}}. \quad (2.33)$$

There are 6 components of the experimental Cauchy stress tensor for the model to predict with two material parameters. However, $T_{13} = T_{31} = 0$ due to simple shear deformation only on one direction, and T_{22} directly equal to applied pressure P , there are only 3 distinct components left to help determine the material parameters.

A cost function has been utilized to determine the material parameters in the following form

$$C(T_{ij}) = \alpha(T_{12_{model}} - T_{12_{exp}})^2 + \beta(T_{11_{model}} - T_{11_{exp}})^2 + \kappa(T_{33_{model}} - T_{33_{exp}})^2, \quad (2.34)$$

where $\mathbf{T} = T_{ij}\mathbf{e}_i \otimes \mathbf{e}_j$. α, β and κ are three weight factors that are introduced in order to tune the material parameter according to the type of flow in subject. In this case, the weight factors has been decided as $\alpha = 3$, $\beta = 1$ and $\kappa = 1$ to approximate the stresses generated in the shear direction with less deviation from the experimental results compared to the other two stress components since it is the most important stress component in the simple shear case. The optimization of two material parameters and predictions of the model versus experimental results are presented in the following figures with respect to the shape ratio r_g . The results start from a shape ratio of 0 which is the spherical grain case and available up to the shape ratio of 0.5 for oblate particles.

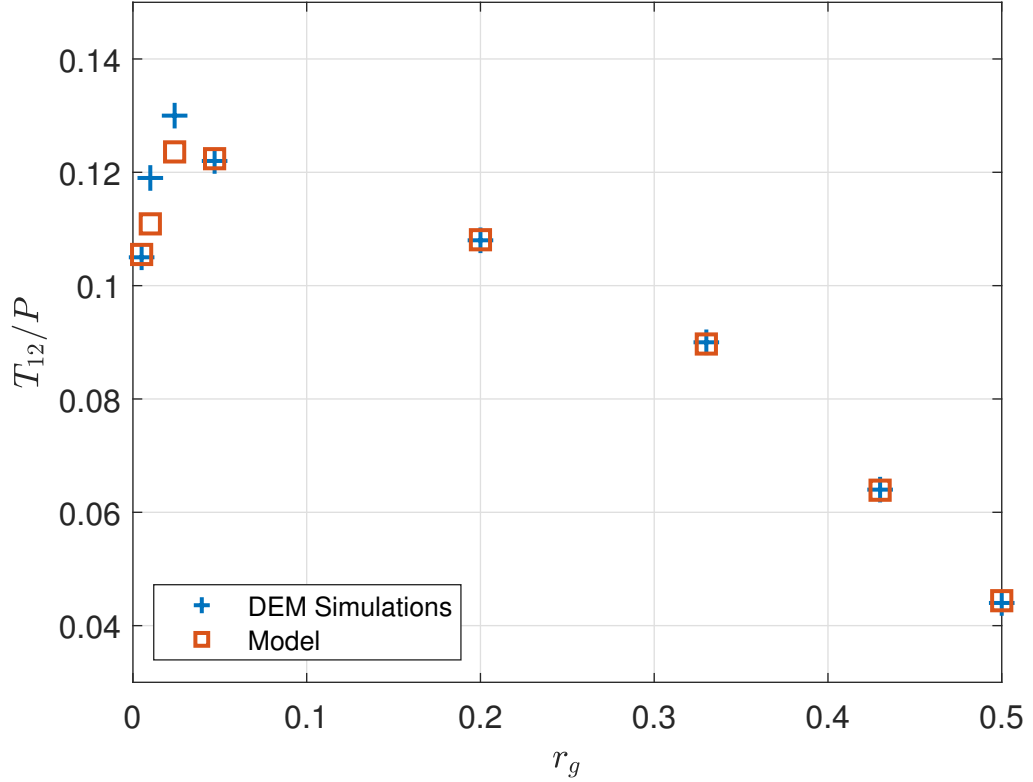


Figure 2.1: Stress component T_{12} versus the shape ratio r_g

It can be seen that in figure 2.1 the model is well predicting the non-monotonous behaviour observed in the stress generated along the shear direction. Also, the model is well capable of capturing stresses generated normal to the shear plane when the deviation of the grains is relatively small. Some deficit has been observed in the stress predictions as the grains become more and more elongated in figures 2.2 and 2.3, but the deficit is only 9.7 percent in the worst case. It should be noted that a better material parameter optimization can be achieved by altering the cost function to reduce the deficit seen in the stress component T_{11} and T_{33} , such as reducing the weight factor of the shear direction stress. Furthermore, as the results of the experimental Cauchy stresses are extracted from an open literature journal paper, it should be admitted that there might be errors involved during this process. A better comparison between the model and experimental results can be achieved when the data is available explicitly from the experimentalist scientists. The most important objective of the model was to capture the non-monotonic behaviour of the stresses generated in the low inertial number (I) case which the model well captured.

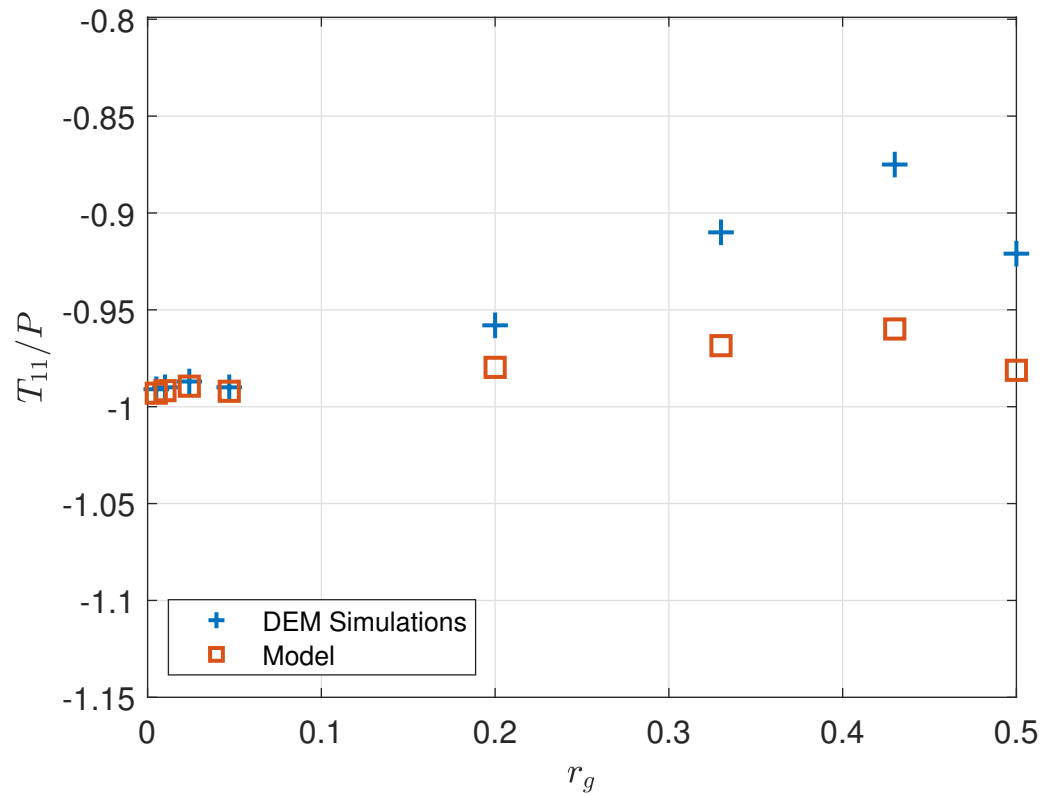


Figure 2.2: Stress component T_{11} versus the shape ratio r_g

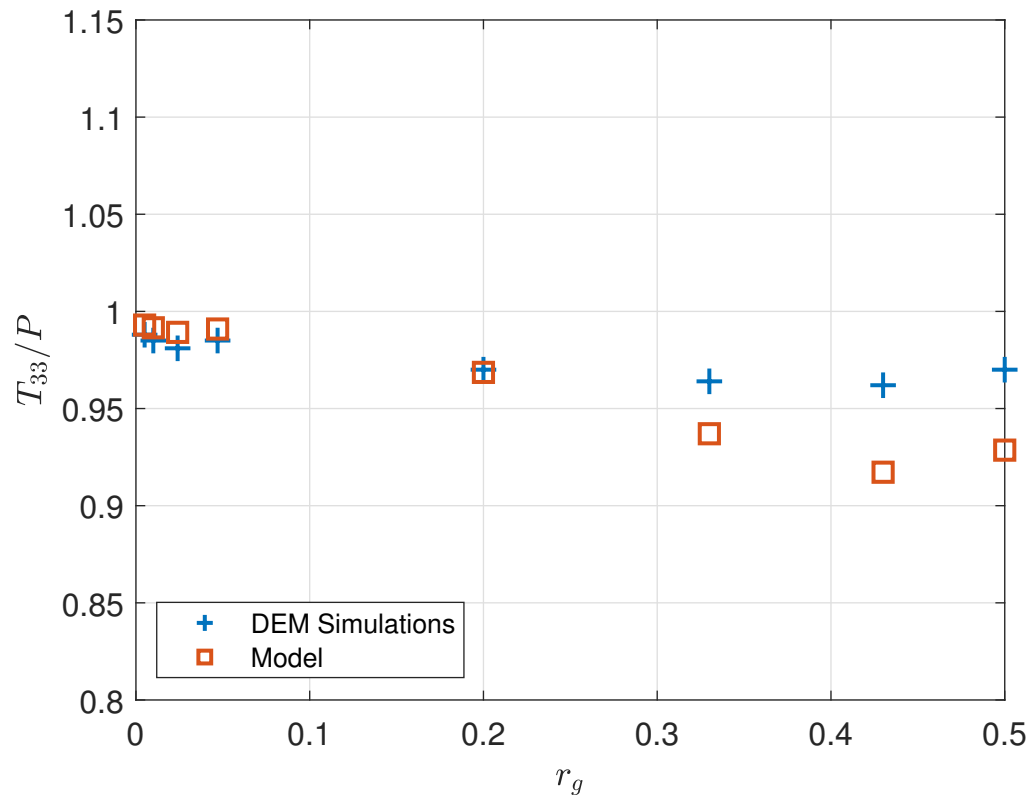


Figure 2.3: Stress component T_{33} versus the shape ratio r_g

As the dissipation inequality asserted that ϕ must be greater than 0 and η to be not less than -0.5, it can be seen in the figure 2.4 that ϕ is satisfying the inequality but η is violating in the cases when the grains are very elongated. Moreover, it has been observed that ϕ is monotonically increasing as the grains become more elongated, and η is monotonically decreasing (see figure 2.4). These outcomes align with what was interpreted earlier for the physical interpretation of the material parameters.

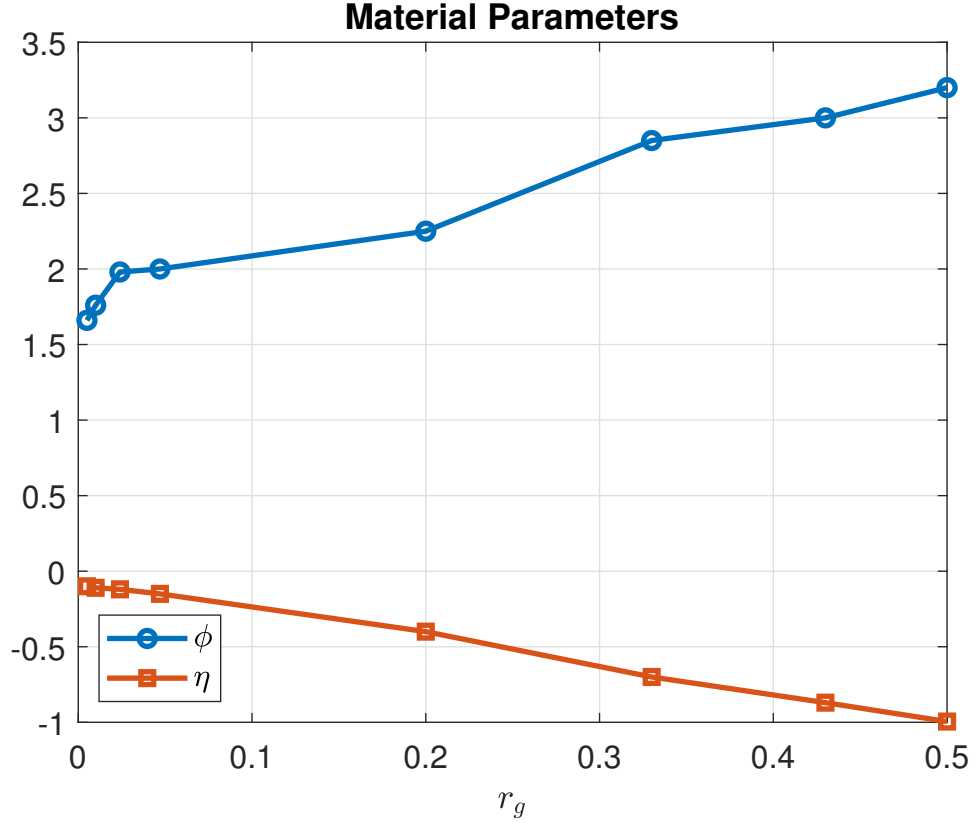


Figure 2.4: Material parameters ϕ and η as a function of shape ratio r_g

The cases where η is smaller than -0.5 when the grains are quite elongated require more attention and further investigation of dissipation inequality. A case where the grains are infinitely elongated, $|r_g| = 1$, and completely aligned with the streamlines of the flow where $|\lambda| \rightarrow 1$ and $|\psi| \rightarrow 0$ the dissipation inequality and shear stress take the following forms

$$P\mu\phi(1 + \eta)\|\mathbf{D}\| \geq 0, \quad (2.35)$$

$$T_{12} = \frac{1}{\sqrt{2}}P\mu\phi(1 + \eta). \quad (2.36)$$

In this special case the dissipation inequality is satisfied when $\eta \geq -1$. Also, the shear stress should be relatively small for the frictionless grains which happens when $\eta = -1$. Therefore, altered dissipation inequality restriction suggests that η can be less than -0.5 . However, it is important to state that the loosened restriction might violate the dissipation inequality. Additional to dissipation inequality restrictions there are others that constitutive laws must obey.

2.3.1 Tensorial Consistency

Tensorial consistency asserts that the Eulerian Cauchy stress tensor \mathbf{T} can only be equal to tensor valued expressions that resolve naturally on the Eulerian basis that the Cauchy stress tensor is defined. In other words, the Eulerian Cauchy stress tensor cannot be equal to a two-point (mixed) or a referential tensor. Since \mathbf{A} , \mathbf{D} and \mathbf{I} are objective Eulerian (spatial) tensors, the tensorial consistency is satisfied.

2.3.2 Dimensional Consistency

Another restriction is posed by the dimensional consistency. The dimension of the stress is $(L)^{-1}M(T)^{-2}$, therefore the right hand side of equation (2.29) must also have the same dimension. Since \mathbf{A} , $\mathbf{D}/\|\mathbf{D}\|$, \mathbf{I} , $\mu(I)$, ϕ and η are dimensionless, and P has the dimension of $(L)^{-1}M(T)^{-2}$, the dimensional consistency is satisfied.

The model was able to predict the non-monotonic behaviour of stresses, however, the comparison could only be done for one instant in time when the flow is in steady-state due to the unavailability of experimental results. To completely reveal the capabilities of the model, a transient problem is needed. Therefore, it has been decided to solve a transient problem and compare the result with experimental results if there is any available. The formulation and the details of the problem have been discussed in the upcoming chapter 3.

Chapter 3

Shear Reversal Problem

To test and reveal the capabilities of the constitutive law, a two-dimensional simple shear problem is selected. The problem starts with grains that are randomly oriented (isotropic distribution visualized in figure 3.1) where the eigenvalues of the tensor \mathbf{A} are 0.5. Then, grains are sheared in one direction until they reach the steady-state where the orientation of the flow is no longer changing in time (visualized in figure 3.2). During the deformation, rheological properties and mechanical response of the flow are calculated. The simple shear problem is selected since it is a transient problem which should capture the fundamentals of the constitutive law, and at the same time simple enough to implement with the available time and resources.

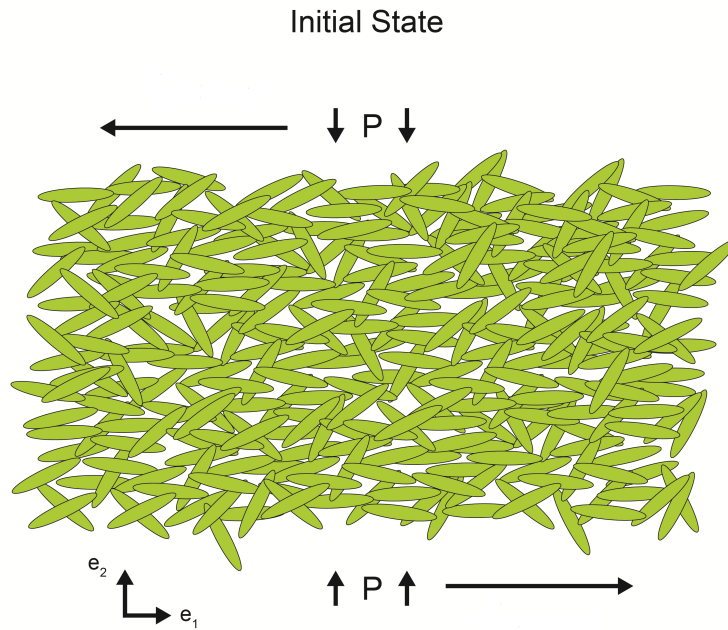


Figure 3.1: Initial state of the problem

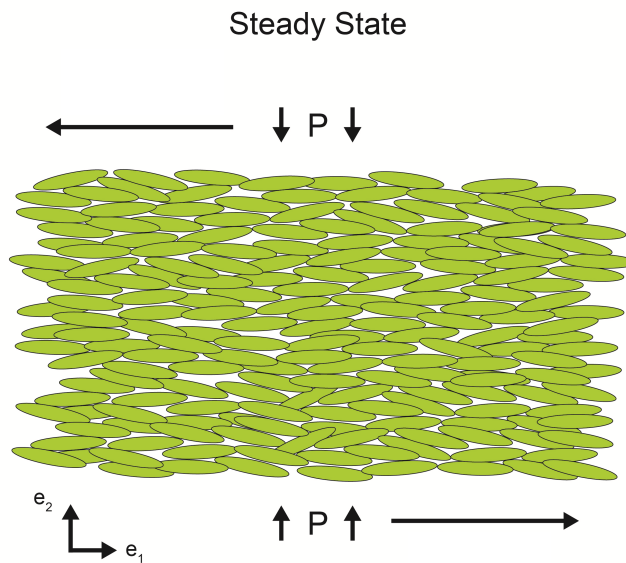


Figure 3.2: Steady-state of the problem when the orientation of the grains are no longer changing in time

To solve a 2-D problem, the model should be converted into 2-D, and material parameters need to be determined accordingly. The following section discusses the details and the process of converting the model into the 2-D form.

3.1 Model Evolution to 2-D

The alterations are needed in the deviatoric part of the stress tensor. The 3-D form of the model was

$$\mathbf{T} = -P\mathbf{I} + P\mu(I)\phi(r_g)(\bar{\mathbf{D}} + \eta(r_g)(\bar{\mathbf{D}}\mathbf{A} + \mathbf{A}\bar{\mathbf{D}} - 2/3(\bar{\mathbf{D}} \cdot \mathbf{A})\mathbf{I})). \quad (3.1)$$

Where $\bar{\mathbf{D}}$ is the rate of deformation tensor divided by the norm of it

$$\bar{\mathbf{D}} = \frac{\mathbf{D}}{\|\mathbf{D}\|}, \quad (3.2)$$

and \mathbf{A}^{dev} is the deviatoric part of the structural tensor

$$\mathbf{A}^{\text{dev}} = \mathbf{A} - \frac{\mathbf{I}}{3}. \quad (3.3)$$

The term $2/3(\bar{\mathbf{D}} \cdot \mathbf{A})\mathbf{I}$ is designed to remove the trace of the term $\bar{\mathbf{D}}\mathbf{A} + \mathbf{A}\bar{\mathbf{D}}$ since the deviatoric part of the stress tensor is designed to be traceless. The trace of the $\bar{\mathbf{D}}\mathbf{A} + \mathbf{A}\bar{\mathbf{D}}$ is equal to $2(\bar{\mathbf{D}} \cdot \mathbf{A})$. Since the trace is a scalar, it is converted into the tensor form with the help of the identity tensor \mathbf{I} . Then the term is divided by 3 because the trace of the identity tensor is 3 where the need is $\text{tr} = 1$. In the case of 2-D, the trace of the identity tensor is 2. Hence the term $2(\bar{\mathbf{D}} \cdot \mathbf{A})\mathbf{I}$ divided by 2, and the term $(\bar{\mathbf{D}} \cdot \mathbf{A})\mathbf{I}$ obtained. Also, the form 3.3 converted as

$$\mathbf{A}^{\text{dev}} = \mathbf{A} - \frac{\mathbf{I}}{2} \quad (3.4)$$

since the trace of 1 needs to be removed from two diagonal components of the tensor \mathbf{A} . Then the 2-D version of the model is

$$\mathbf{T} = -P\mathbf{I} + P\mu(I)\phi(r_g)(\bar{\mathbf{D}} + \eta(r_g)(\bar{\mathbf{D}}\mathbf{A} + \mathbf{A}\bar{\mathbf{D}} - (\bar{\mathbf{D}} \cdot \mathbf{A})\mathbf{I})). \quad (3.5)$$

3.2 Material Parameters for 2-D Problem

To determine the material parameters, the same procedure as described in section 2.3 has been followed. The experimental results were obtained from Trulsson's [25] 2-D DEM simple shear study where he reported the director tensor and the associated stresses. The director tensor \mathbf{R} is converted into tensor \mathbf{A} by

$$\mathbf{R} = 2\mathbf{A} - \mathbf{I}. \quad (3.6)$$

In this problem, grains with the shape ratio $r_g = 0.5$ (aspect ratio 3) with 0.4 interparticle friction coefficient (μ_s) are selected since the shape ratio of 0.5 falls into moderately elongated grain category and 0.4 interparticle friction coefficient is used by the majority of researcher who studied the rheology of the granular materials. After obtaining the material parameters, $\lambda = 0.77$ and $\psi = 0.31$, from the empirical relations that [18] proposed and orientation tensor \mathbf{A} from experimental DEM results, components of the stress tensor extracted using the pressure rescaled normal stress difference parameter N_1/P that Trulsson [25] reported. To determine the stress model material parameters ϕ and η , the cost function (2.34) has been used. The cost function optimization revealed that the 2-D model was not able to capture the experimental stresses in the case of the simple shear. It has been quickly realized that the diagonal components of the proposed model are restricted to be equal to the pressure such that

$$T_{11} = T_{22} = -P, \quad (3.7)$$

at all times. It was evident that the elimination of the 3rd dimension removed the richness of the proposed model. Hence it became incapable of capturing the anisotropic granular rheology. Before adding extra terms that are presented using the isotropic representation theorem two relatively easier changes have been investigated to regain the lost anisotropic richness of the model. The first one was to use the tensor \mathbf{A} to remove the trace of the term $\bar{\mathbf{D}}\mathbf{A} + \mathbf{A}\bar{\mathbf{D}}$ instead of using identity tensor \mathbf{I} . The following form

$$\mathbf{T} = -P\mathbf{I} + P\mu(I)\phi(\bar{\mathbf{D}} + \eta(\bar{\mathbf{D}}\mathbf{A} + \mathbf{A}\bar{\mathbf{D}} - (\bar{\mathbf{D}} \cdot \mathbf{A})\mathbf{A})), \quad (3.8)$$

also was not able to capture the experimental results due to the same issue of having no freedom over the diagonal components of the model. The second idea was to use

the deviatoric part (\mathbf{A}^{dev}) of the tensor \mathbf{A} instead of itself in the model. The change brought the model into

$$\mathbf{T} = -P\mathbf{I} + P\mu(I)\phi(\bar{\mathbf{D}} + \eta(\bar{\mathbf{D}}\mathbf{A}^{\text{dev}} + \mathbf{A}^{\text{dev}}\bar{\mathbf{D}} - (\bar{\mathbf{D}} \cdot \mathbf{A}^{\text{dev}})\mathbf{I})). \quad (3.9)$$

Replacing \mathbf{A} by \mathbf{A}^{dev} only shifted the predictions since $\mathbf{A} = \mathbf{A}^{\text{dev}} - \mathbf{I}/2$ which did not solve the problem. After experiencing that the relatively easy alterations are not addressing the issue, it has been decided to add an another term to the model to capture the anisotropy again.

Then the previously disregarded term $\nu(rg, f)\|\mathbf{D}\|\mathbf{A}^{\text{dev}}$ due to the dissipation inequality decided to be brought back to the model. The added term brought the model into form.

$$\mathbf{T} = -P\mathbf{I} + P\mu(I)\phi(\bar{\mathbf{D}} + \eta(\bar{\mathbf{D}}\mathbf{A} + \mathbf{A}\bar{\mathbf{D}} - (\bar{\mathbf{D}} \cdot \mathbf{A})\mathbf{I}) + \nu\|\mathbf{D}\|\mathbf{A}^{\text{dev}}). \quad (3.10)$$

In the 2-dimensional simple shear case the Cauchy stress tensor has three independent variables which are T_{11} , T_{22} and T_{12} . However, a closer look at the structure of the proposed model reveals that there are only two independent parameters which are T_{12} and the difference in normal stresses $T_{11} - T_{22}$. Since $T_{11} = -P + \tau_{11}$ and $T_{22} = -P + \tau_{22}$, the only difference between the two components is the deficit in the deviatoric part of stress. Hence only the difference between the diagonal components of the stress tensor model is independent. Therefore, the phenomenological model only needs to satisfy 2 independent equations. The addition of the 3rd term with an extra material parameter ν causes an incident that the model has 3 independent material parameters to capture 2 independent variables. The redundancy in this situation brings about the question of how the model parameters can be determined. To avoid that the model decided to be limited to only two material parameters. Since \mathbf{A} is capturing the orientation of the grains and η is interpreted as the reduction in the shear resistance due to alignment characteristic of the grains, it has been decided to take

$$\nu = \eta \quad (3.11)$$

to reduce the number of the material parameters to two. Then the 2-D phenomenological model reached to the form

$$\mathbf{T} = -P\mathbf{I} + P\mu(I)\phi(\bar{\mathbf{D}} + \eta(\bar{\mathbf{D}}\mathbf{A} + \mathbf{A}\bar{\mathbf{D}} - (\bar{\mathbf{D}} \cdot \mathbf{A})\mathbf{I} + \|\mathbf{D}\|\mathbf{A}^{\text{dev}})). \quad (3.12)$$

The addition of another term requires a revisit to the dissipation inequality to establish the restrictions that are posed by the laws of physics. For equation (3.12) the dissipation inequality posed the following two restrictions

$$\phi \geq 0, \quad (3.13)$$

$$\frac{1}{\|\mathbf{D}\|}(\mathbf{I} + 2\eta\mathbf{A}) \cdot \mathbf{D}^2 + \eta(\mathbf{A}^{\text{dev}} \cdot \mathbf{D}) \geq 0. \quad (3.14)$$

Unfortunately in this case the dissipation inequality cannot be further simplified to obtain a direct requirement for the η , therefore equation (3.14) must be calculated for all points in space at every instant of time throughout the problem to ensure that the dissipation inequality is not violated. The new form of the 2-D model was able to capture the experimental stresses reported in [25]. The table 3.1 presents the results of the optimization of the cost function (2.34) and table 3.2 summarizes the material parameters for this problem.

Table 3.1: Material Parameter Fit Results

Stress Components	T_{11}	T_{12}	T_{22}
DEM	-1.14	-0.49	-1
Model	-0.93	-0.49	-0.80
Error Percentage	%22	%0	%20

Table 3.2: Material Parameters

Material Parameters	Dimensionless value
λ	0.77
ψ	0.31
ϕ	4.01
η	-0.26

The results suggest that the proposed model predicts the experimental results better in 3-D form. However, since the real-life problems of granular materials is mostly 3-D. Hence, slightly less accurate predictions did not raise a concern.

3.3 Governing Equations and the Procedure of Solving the Problem

As all 4 material parameters are determined for the constitutive laws of \mathbf{A} and \mathbf{T} , only the material constants left are related to the term $\mu(I)$. The following form of $\mu(I)$ which is proposed by [9] is used in this problem.

$$\mu(I) = \mu_s + \mu_1 I^\alpha \quad (3.15)$$

Since the interest of this study is the flow of the grains when $I \rightarrow 0$, $\mu(I)$ has the form

$$\mu(I) = \mu_s, \quad (3.16)$$

where μ_s is the effective friction coefficient for the spherical frictionless particles, and it is extracted as 0.4 for this problem from [25].

Then the constitutive law for 2-D stresses has the form

$$\frac{\mathbf{T}}{P} = -\mathbf{I} + \mu_s \phi [\bar{\mathbf{D}} + \eta(\bar{\mathbf{D}}\mathbf{A} + \mathbf{A}\bar{\mathbf{D}} - (\bar{\mathbf{D}} \cdot \mathbf{A})\mathbf{I} + \|\mathbf{D}\|\mathbf{A}^{\text{dev}})]. \quad (3.17)$$

3.3.1 Governing Equations

Euler's linear and angular momentum balance equations and the mass balance (conservation of mass) equation are enough to fully describe the motion of the continua.

3.3.1.1 Mass Balance

The Eulerian form of the conservation of mass is given as

$$\dot{\rho} + \rho \operatorname{div} \mathbf{v} = 0. \quad (3.18)$$

In this problem the material assumed to be incompressible and can only undergo isochoric motions. Hence density change $\dot{\rho} = 0$, and $\operatorname{tr} \mathbf{D} = I_1(\mathbf{D}) = \operatorname{div} \mathbf{v} = 0$ since they are the measure of pure dilation they must be equal to 0 for the incompressible case. One can also show that for the volume preserving flow $\dot{J} = J \operatorname{div} \mathbf{v} = 0$ where J is the Jacobian, therefore $\operatorname{div} \mathbf{v}$ must be equal to 0 to satisfy the positivity of the Jacobian J . In this case, the mass balance equation does not provide any usable equation to solve for P , \mathbf{A} , and \mathbf{v}

3.3.1.2 Linear Momentum Balance

The Eulerian form of the linear momentum balance is given as

$$\rho \dot{\mathbf{v}} = \rho \mathbf{b} + \text{div } \mathbf{T}, \quad (3.19)$$

where \mathbf{b} is the body forces. In this problem, the gravity is neglected and since there are no other body forces acting on the continua, $\mathbf{b} = 0$.

The material derivative of the velocity vector \mathbf{v} is

$$\dot{\mathbf{v}} = \frac{dv}{dt} + (\text{grad } \mathbf{v})\mathbf{v}. \quad (3.20)$$

The grad \mathbf{v} is given by the following expression

$$\text{grad } \mathbf{v} = \mathbf{L} = \frac{\partial v_1}{\partial x_2} \mathbf{e}_1 \otimes \mathbf{e}_2. \quad (3.21)$$

The velocity vector \mathbf{v} has the form

$$\mathbf{v} = v_1 \mathbf{e}_1. \quad (3.22)$$

Therefore, spatial velocity gradient \mathbf{L} operating on the velocity vector \mathbf{v} is

$$\mathbf{L}\mathbf{v} = 0. \quad (3.23)$$

Then the linear momentum balance equation reduces to

$$\rho \frac{dv}{dt} = \text{div } \mathbf{T}. \quad (3.24)$$

The divergence of a differentiable tensor valued function \mathbf{T} is defined as

$$\mathbf{T} = \frac{\partial T_{ij}}{\partial x_j} \mathbf{e}_i. \quad (3.25)$$

Before taking the divergence of the tensor \mathbf{T} , known rate of deformation tensor \mathbf{D} input as

$$\mathbf{D} = \frac{1}{2} \frac{\partial v_1}{\partial x_2} (\mathbf{e}_1 \otimes \mathbf{e}_2 + \mathbf{e}_2 \otimes \mathbf{e}_1), \quad (3.26)$$

$$\|\mathbf{D}\| = \sqrt{\mathbf{D} \cdot \mathbf{D}} = \sqrt{\text{tr } \mathbf{D}^2}, \quad (3.27)$$

$$\|\mathbf{D}\| = \frac{\sqrt{2}}{2} \left| \frac{\partial v_1}{\partial x_2} \right|, \quad (3.28)$$

$$\frac{\mathbf{D}}{\|\mathbf{D}\|} = \bar{\mathbf{D}} = \begin{cases} \frac{\sqrt{2}}{2}(\mathbf{e}_1 \otimes \mathbf{e}_2 + \mathbf{e}_2 \otimes \mathbf{e}_1) & \text{when } \partial v_1 / \partial x_2 > 0 \\ \frac{-\sqrt{2}}{2}(\mathbf{e}_1 \otimes \mathbf{e}_2 + \mathbf{e}_2 \otimes \mathbf{e}_1) & \text{when } \partial v_1 / \partial x_2 < 0 \\ \mathbf{0} & \text{when } \partial v_1 / \partial x_2 = 0. \end{cases} \quad (3.29)$$

The linear momentum balance equation 3.24 in components form provides 2 equations to solve for P , \mathbf{A} and \mathbf{v} . The equations are

$$0 = -\frac{\partial P}{\partial x_2} + \mu_s \phi \eta \left[\frac{\partial P}{\partial x_2} A_{22} + P \frac{\partial A_{22}}{\partial x_2} - \frac{\partial P}{\partial x_2} \frac{1}{2} \right] \quad (3.30)$$

and

$$\rho \frac{\partial v}{\partial t} = \frac{\mu_s \phi}{\sqrt{2}} \frac{\partial P}{\partial x_2} + \frac{\mu_s \phi \eta}{\sqrt{2}} \left[\frac{\partial P}{\partial x_2} A_{22} + P \frac{\partial A_{22}}{\partial x_2} + \frac{\partial P}{\partial x_2} A_{11} + P \frac{\partial A_{11}}{\partial x_2} \right] + \mu_s \phi \eta \left[\frac{\partial P}{\partial x_2} A_{12} + P \frac{\partial A_{12}}{\partial x_2} \right]. \quad (3.31)$$

There are 5 unknowns in these equations which are pressure P , components of the tensor \mathbf{A} (A_{11}, A_{12}, A_{22}) and velocity vector \mathbf{v} . 5 unknowns require 5 equations to complete the system of equations for a unique solution. The remaining equations are provided by the constitutive law that gives the evolution of \mathbf{A} .

3.3.1.3 Equations from Evolution of \mathbf{A}

The evolution of \mathbf{A} is converted into the 2-D form as

$$\dot{\mathbf{A}} = \mathbf{W}\mathbf{A} - \mathbf{A}\mathbf{W} + \lambda(\mathbf{D}\mathbf{A} + \mathbf{A}\mathbf{D} - 2(\mathbf{A} : \mathbf{D})\mathbf{A}) - \psi\|\mathbf{D}\|(\mathbf{A} - \mathbf{I}/2). \quad (3.32)$$

The left hand side of the equation is

$$\dot{\mathbf{A}} = \frac{\partial \mathbf{A}}{\partial t} + (\text{grad } \mathbf{A})\mathbf{v}. \quad (3.33)$$

The $\dot{\mathbf{A}}$ constitutive law does not contain any gradient term on the right hand side. Hence there is no dependency on the $\text{grad}(\mathbf{A})$ in the evolution of the orientation of

the grains. Hence,

$$(\text{grad } \mathbf{A})\mathbf{v} = \mathbf{0}. \quad (3.34)$$

The rearranged version of the equation (3.32) in the components form gives the following 3 equations to complete the system of equations for a solution.

$$\frac{\partial A_{11}}{\partial t} = \frac{\partial v}{\partial x_2} \left[A_{12} + \lambda A_{12} - 2\lambda A_{12} A_{11} - \frac{\psi}{\sqrt{2}} A_{11} + \frac{\psi}{2\sqrt{2}} \right] \quad (3.35)$$

$$\frac{\partial A_{12}}{\partial t} = \frac{\partial v}{\partial x_2} \left[\frac{A_{22}}{2} - \frac{A_{11}}{2} + \frac{\lambda}{2} (A_{11} + A_{22}) - 2\lambda A_{12}^2 - \frac{\psi A_{12}}{\sqrt{2}} \right] \quad (3.36)$$

$$\frac{\partial A_{22}}{\partial t} = \frac{\partial v}{\partial x_2} \left[-A_{12} + \lambda A_{12} - 2\lambda A_{12} A_{22} - \frac{\psi}{\sqrt{2}} A_{22} + \frac{\psi}{2\sqrt{2}} \right] \quad (3.37)$$

Equations (3.35) to (3.37) and (3.30-3.31) are valid when $\partial v_1 / \partial x_2 > 0$. For the case when $\partial v_1 / \partial x_2 < 0$ equations are provided in the appendix A.1.

3.3.1.4 Initial Conditions

The grains are at isotropic distribution at all points in space which gives

$$\mathbf{A} = \frac{1}{2}(\mathbf{e}_1 \otimes \mathbf{e}_1 + \mathbf{e}_2 \otimes \mathbf{e}_2). \quad (3.38)$$

The initial pressure at all points are taken to be equal to the applied boundary pressure $P_{boundary} = 0.1$. Grains are given a non-zero initial velocity field with linear spatial velocity gradient at all points to avoid the situation where $\bar{\mathbf{D}} = \mathbf{0}$. The velocities at the boundaries are taken as $V_{bottom} = 1$ and $V_{top} = -1$. The figure 3.3 illustrates the initial velocity field.

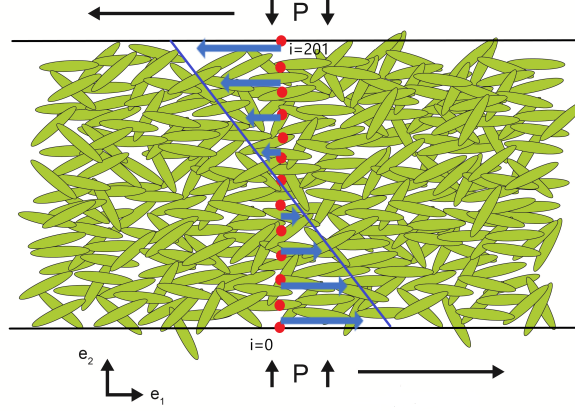


Figure 3.3: Mesh and Initial Velocity Field Display

3.3.1.5 Boundary Conditions

The no-slip condition at the top and bottom boundaries is assumed. At the boundaries the velocity of the particles are taken to be equal to the moving boundary velocity.

$$V_{boundary} = V_{particles} \quad (3.39)$$

The pressure of the grains at the boundary is equal to the traction at the boundary. The stress normal to the shear plane is given by the following expression

$$\mathbf{e}_2 \cdot \mathbf{T}\mathbf{e}_2 = P_{boundary} = -P + P\mu\phi\eta(A_{22} - \frac{1}{2}). \quad (3.40)$$

3.3.1.6 Finite Difference Approximations

The first order derivatives in the partial differential equations are approximated by the finite difference method. Approximations are done by using second order approximation of first order derivatives. The forward finite difference formula is given as

$$f'(x) = \frac{-f(x_{i+2}) + 4f(x_{i+1}) - 3f(x_i)}{2h} + \mathcal{O}(h^2). \quad (3.41)$$

The backward finite difference is

$$f'(x) = \frac{3f(x_i) - 4f(x_{i-1}) - f(x_{i-2})}{2h} + \mathcal{O}(h^2), \quad (3.42)$$

and the central finite difference is

$$f'(x) = \frac{f(x_{i+1}) + f(x_{i-1})}{2h} + \mathcal{O}(h^2). \quad (3.43)$$

The problem is approximated by explicit finite difference scheme where the time derivative of the velocity vector is known in the previous time step, and the next time step is explicitly depends on the previous time step. Hence the time derivative

$$\frac{\partial v}{\partial t} = \frac{v_i^{j+1} - v_i^j}{\Delta t} \quad (3.44)$$

where i represents discretization in space and j represents discretization in time. The quantities $X_i = V_i, P_i, A_{11i}, A_{22i}, A_{12i}$ are known at time $j=0$, and the next time step is calculated by time integration.

3.4 Results

As discussed earlier, the grains were given a linear initial velocity field. The top and the bottom boundary velocities were kept constant throughout the flow. Since there is no slip at the boundaries are assumed, the velocity field of the flow was constant throughout the deformation. The figure 3.4 presents the velocity field that has been chosen. The velocity of the grains was checked over throughout the deformation to make sure there is no other contributor that causes a change in the velocity field, such as pressure or the orientation of the grains. The velocity of the grains has been monitored as a feedback parameter to understand if the solution of the system of equations is valid.

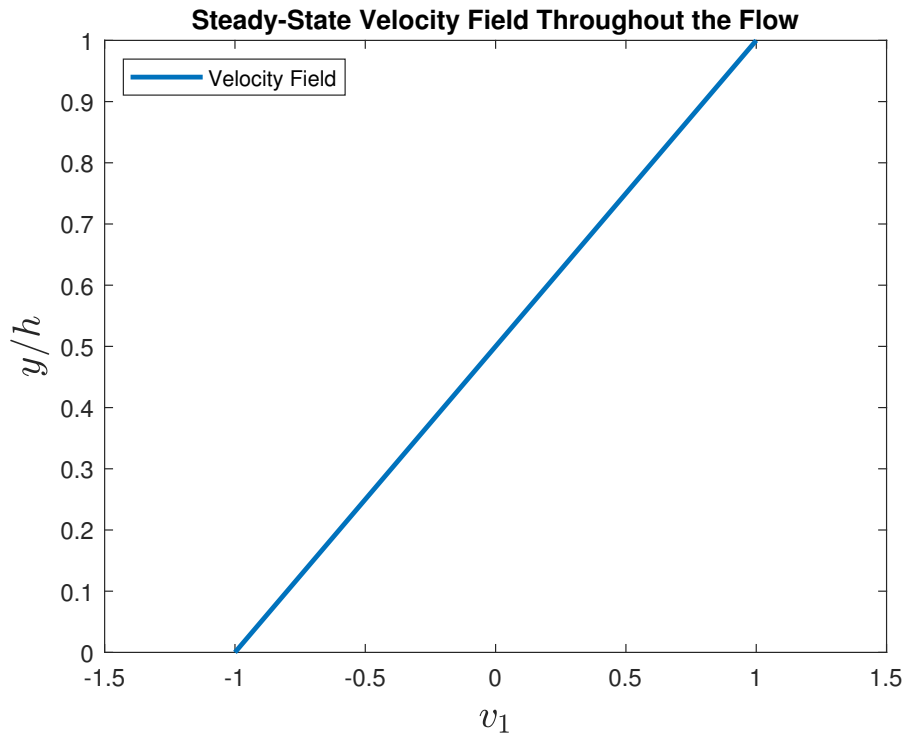


Figure 3.4: Velocity of the grains versus the relative position in the vertical axis of the flow where h is the flow height and y is the position in the flow height

3.4.1 Mechanical Response of the System

To study the mechanical response of the system, 3 different grains have been selected. The first grains are the spherical ones with the shape ratio of 0. They are selected to reveal the effect of the grain orientation between the elongated grains and spherical. Secondly, grains with the shape ratio of 0.5 has been picked in order to demonstrate high self-ordering characteristics and interlocking behaviour. Lastly, grains with the shape ratio of 0.2 has been studied to show the behaviour of relatively low self-ordering and tangling characteristic. 3 picks have been made to show the mechanical behaviour of the tails of the grain spectrum as well as the midpoint of those two tails. Since the flow is simple shear in one direction, the behaviour of the stress component T_{12} which is the shear stress in the shear direction is investigated. According to Nagy [19] and Trulsson [25], highly elongated grains are easier to shear in low inertial number steady-state flow, and between the shape ratio's of 0.005 to 0.33 the grains are harder to shear compared to spherical ones. In this problem, the constitutive law was able to capture this behaviour. It can be seen in the figure 3.5 that after the dimensionless time $\hat{t} = 1.1$ where the flow is at steady-state, the shear

stress component T_{12} is higher for the grains with the shape ratio of 0.2 compared to spherical grains which have the shape ratio of 0. Also, the grains with higher elongation, the shape ratio of 0.5, are the easiest to shear compared to the other two. The shear stresses generated with the spherical grains is not changing in time since there is no self-orientation with the flow or change in interlocking behaviour in time. The stress response model's material parameters are $\phi = 1$ and $\eta = 0$ for the spherical case which boils down the model to the original $\mu(I)$ rheology.

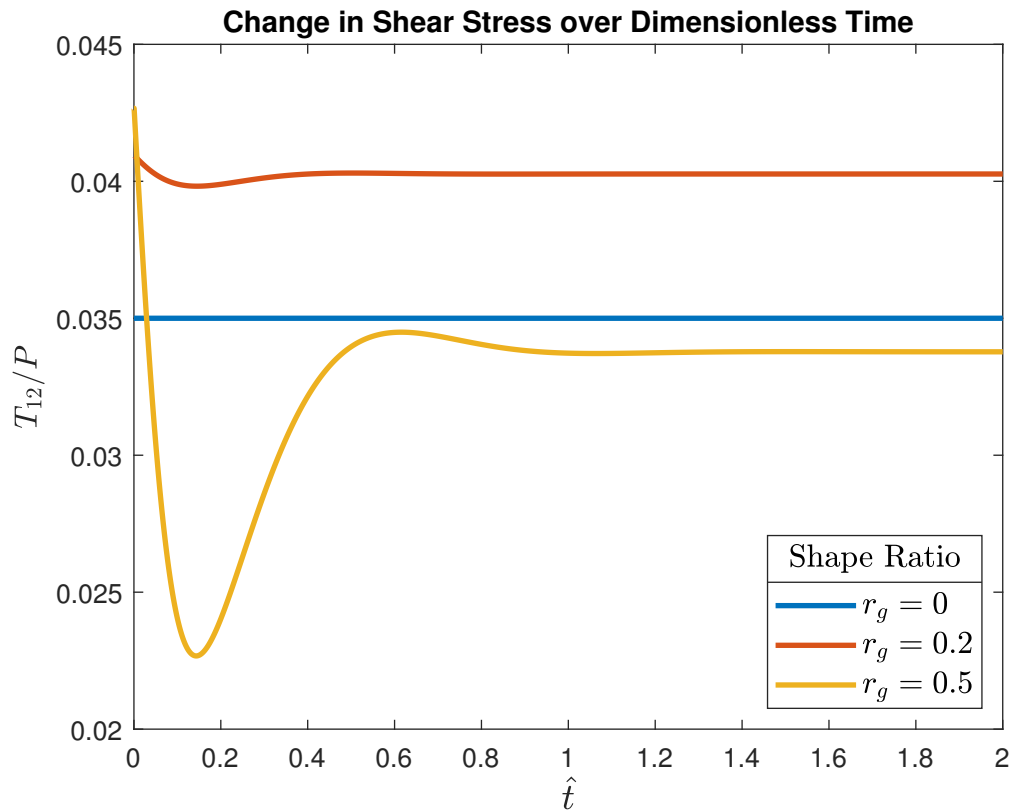


Figure 3.5: Normalized shear stress at the walls versus dimensionless time $\hat{t} = t|\dot{\gamma}|$

The change in shear stress in time as the grains orient themselves in the flow with respect to the streamlines is the main interest of this study. As discussed earlier, two material parameters are interpreted as they govern the tangling and the ability to orient with the flow behaviour of the grains. As the grains become more and more elongated, it has been interpreted that both tangling behaviour and the ability to orient with the flow increases, but the competition between the two effects could not be interpreted due to the lack of experimental data availability. The study with the

grains that have the shape ratio of 0.5 revealed the competing effects on the stress response of the flow quite clearly. It can be seen figure 3.5 that the shear stress of the highly elongated grains decreases steeply as the grains orient themselves with respect to the streamlines of the flow. The effect of the increased tangling compared to the spherical grains starts to show its contribution after the dimensionless time $\hat{t} = 0.2$ and increases the shear stress. Figure 3.6 reveals when the decrease and the increase in shear stress happen with respect to the A_{11} component of the structural tensor which is along the dominant alignment axis of the flow. The shear stress decreases as more and more grains align with the streamlines up to $A_{11} = 0.7$, then slightly increases as the grains continue to align themselves in the flow direction.

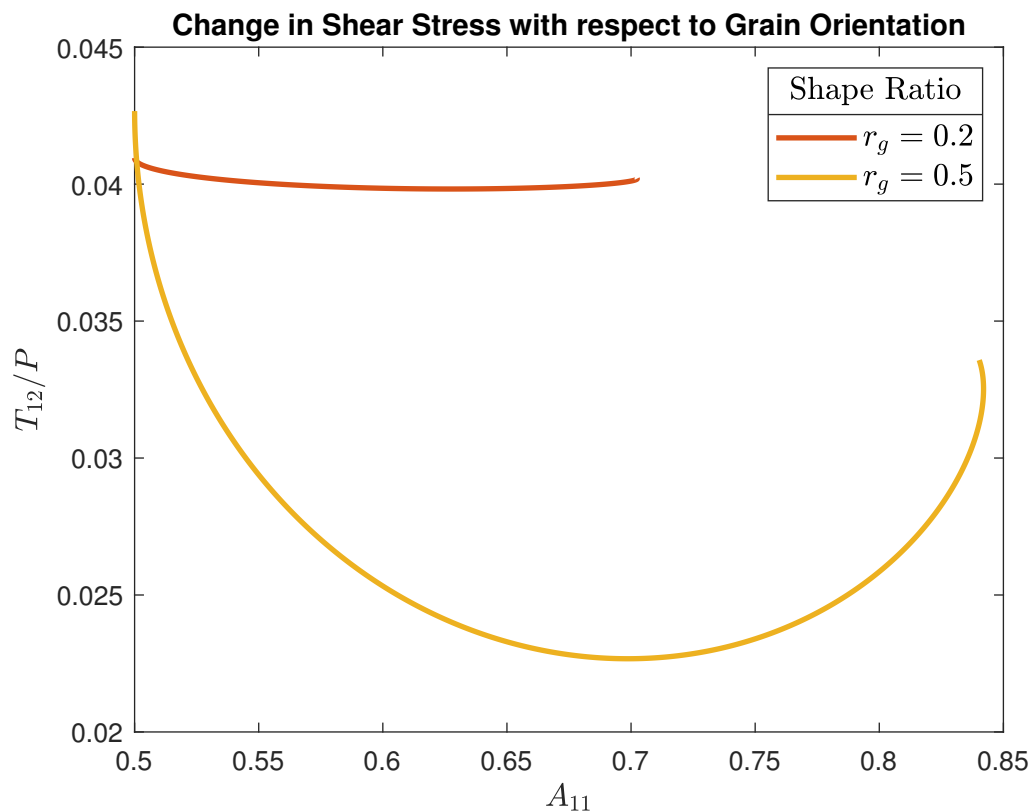


Figure 3.6: Normalized shear stress with respect to A_{11}

On the other hand, grains with the shape ratio of 0.2 demonstrates the two effect in much more mild sense. The shear stress follows a similar trend as the highly elongated grains. The shear stress decreases as the grains align themselves with the streamlines but the decrease is much less since they do not have the same strong ability to orient themselves. Also, the increase in shear stress after reaching the minimum is much

less compared to highly elongated ones since they also do not have a strong tangling or jamming behaviour. The secondary increase in the shear stress after reaching to a highly ordered state arouse curiosity since that behaviour expected to happen in the beginning of the flow where the grain's orientation is closer to isotropic distribution. A closer look at the stress response model in components form revealed that in this case the shear stress component $T_{12} = P\mu(I)\phi[\eta(1/\sqrt{2} + A_{12}) + 1/\sqrt{2}]$ only depends on the A_{12} component of the structural tensor \mathbf{A} and pressure. The figure 3.7 shows the change in the shear stress with respect to the A_{12} component. At this time, there is no available numerical or experimental data that the shear stress predictions of the model over time can be compared to.



Figure 3.7: Normalized shear stress with respect to A_{12}

3.4.2 Orientation of the Grains

The grains were at isotropic distribution at the initial condition where the eigenvalues of the tensor \mathbf{A} were 0.5. In the 2-dimensional case tensor \mathbf{A} has 3 components that represent the orientation of the grains. In this case, the A_{11} represents the amount

of particles aligned in the direction of the flow. The A_{22} component indicates the number of particles that are aligned perpendicular to the shear plane, and the change in the A_{12} component can be read as the number of particles that are changing its orientation during the flow.

As discussed earlier, higher shape ratio (elongated) particle's ability to orient themselves with the flow streamlines are higher compared to lower shape ratio particles. Figure 3.8 presents the change in the A_{11} component of the structure tensor over time. All 3 different grains are started from 0.5, the isotropic distribution, and reached to steady-state after the dimensionless time $\hat{t} = 1.1$. As expected the grains with the shape ratio of 0.5 aligned themselves faster compared to the shape ratio of 0.2 particles, and reached a higher degree of orientation at the steady-state. At this time, there is no supporting experimental data in the open literature that the more elongated particles align themselves faster compared to less elongated particles. Grains with the shape ratio of 0.5 have reached 0.85 and 0.15 eigenvalues at the steady-state, on the other hand, grains with the shape ratio of 0.2 only reached 0.73 and 0.23. Since the spherical particles do not have an orientation due to shape isotropy, they remain at 0.5 eigenvalues throughout the flow.

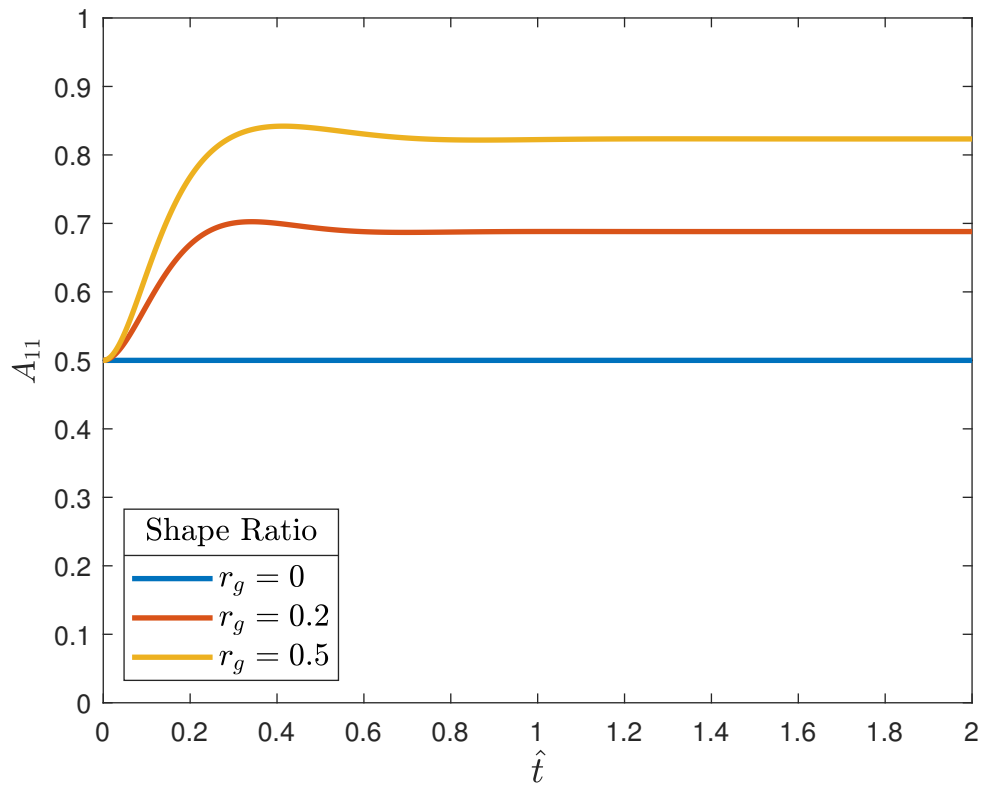


Figure 3.8: A_{11} component of the structural tensor versus dimensionless time $\hat{t} = t|\dot{\gamma}|$

Similar to the A_{11} component of the structure tensor, A_{22} component of the more elongated particles decreases faster meaning that more particles are aligning with the shear direction compared to the less elongated and reaches a lower final value.

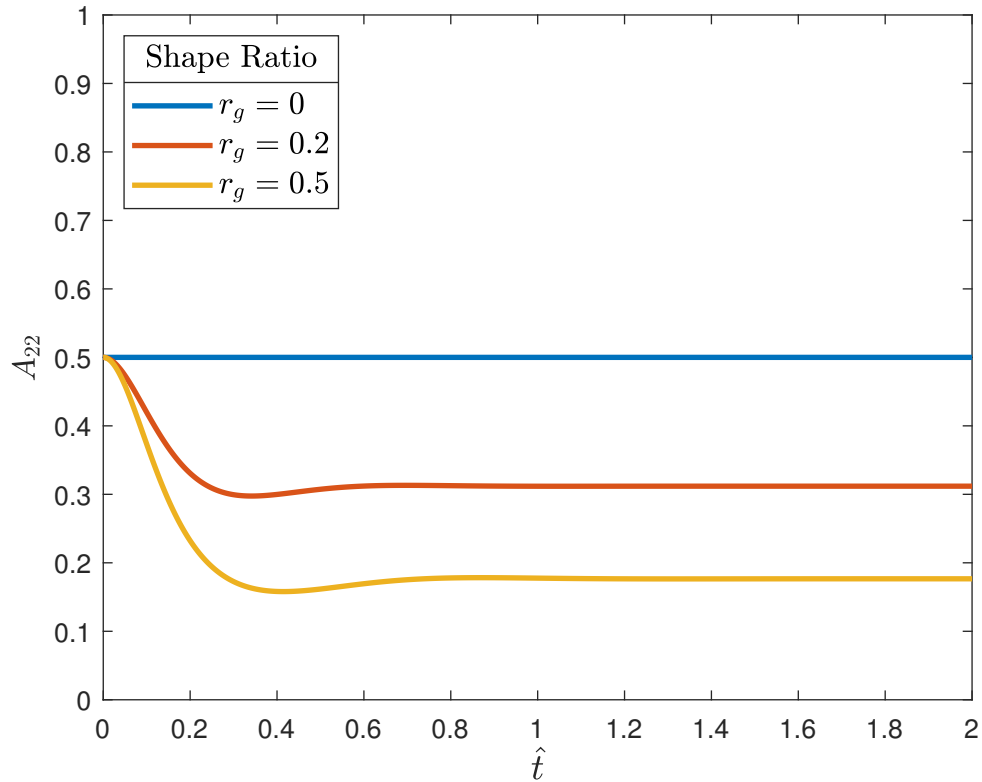


Figure 3.9: A_{22} component of the structural tensor versus dimensionless time $\hat{t} = t|\dot{\gamma}|$

The A_{12} component of the structure tensor is starting from 0 since the initial condition of the grains are the isotropic distribution. The change in A_{12} component over time can be read as the number of particles that are rotating or changing their orientation with the flow. The particles with the ability to orient themselves with the streamlines experience an increase meaning that the particles that are perpendicular to the shear plane are rotating to align with the flow direction. The stronger the ability to orient with the flow yields to a higher A_{12} component meaning that more particles are rotating to self orient themselves with the flow. Hence the increase in the A_{12} component of the shape ratio of 0.5 grains compared to the shape ratio of 0.2 is greater. On the other hand, spherical grains do not experience any change in the A_{12} component due to the shape isotropy of particles.

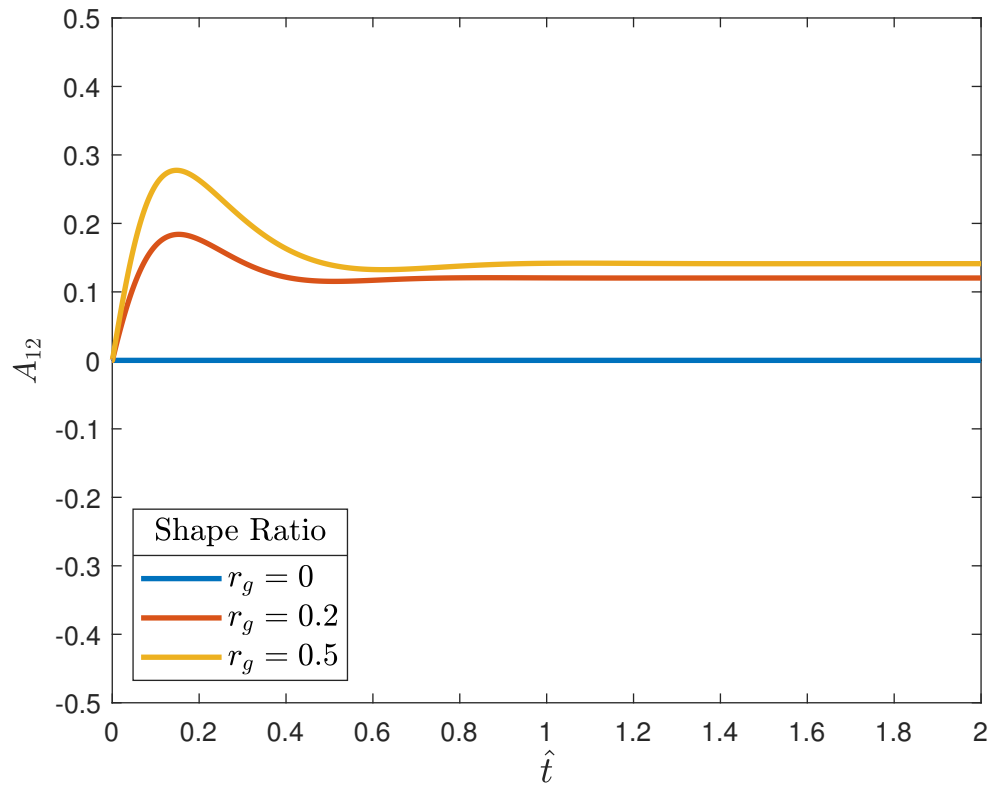


Figure 3.10: A_{12} component of the structural tensor versus dimensionless time $\hat{t} = t|\dot{\gamma}|$

It is important to mention that, both constitutive relations are local which means they only depend on the quantities that are defined at that point. The simple shear problem is a kinematic problem, but there is no change in the velocity of the particles over time. Hence the orientation of the grains is identical throughout the \mathbf{e}_2 . It means that at any instant of time, the structure tensor \mathbf{A} is the same for all the points in the flow.

Chapter 4

Conclusion

The fluid-like behaviour of the granular materials has intrigued scientists and drew attention owing to its rich research potential. The well-received $\mu(I)$ rheology captures the mechanical response and flow characteristics of spherical (shape isotropic) grains when there are no strong spatial gradients of the velocity vector and time derivatives in the system. It has been shown in the open literature that the shape-induced anisotropy of the grains greatly affects the rheological properties and mechanical response of the system [13, 19, 20, 25]. The shape induced anisotropy hinders the utilization of $\mu(I)$ rheology. The interpretation of the available experimental work suggests that two competing factors govern the rheological and mechanical response of the systems. These two effects of the ellipsoidal grains are interpreted as the ability of the grains to align themselves with the flow streamlines and the tangling or interlocking characteristics. The study of the critical viscosity μ_s suggested that the elongated grains exhibit more or less shear resistance compared to spherical grains depending on their shape ratio (aspect ratio). The non-monotonous behaviour of the critical viscosity with the shape ratio supported the idea of the two competing effects on the system's response. Therefore, the grain shape effect was found to be essential to be included in a stress response model. The grain shape affects the system's mechanical response by changing the interactions of the grains in the micro-scale. This change acts upon the orientation of the grains during the flow. It has been discussed that the elongated grains align themselves with respect to the streamlines of the flow with an angle. This average orientation angle found to be sensitive to the grain shape [18, 19, 25]. Hence, the grain shape is affecting the orientation of the grains and this orientation changes the mechanical response of the system. The more randomly oriented grains are harder to shear compared to the grains that are aligned

in the flow direction. Therefore, in addition to the grain shape, the orientation effect of the grains is decided to be included in the response model. The main objective of this study was to propose a constitutive stress model that can capture the grain shape and orientation effect on the mechanical response. The main motivation came from the lack of a constitutive model that can be applied to the shape anisotropic granular materials where the shape cannot be determined by a single variable.

To capture the orientation effect of the grains, the kinematic continuum model proposed by Nadler and Einav [18] has been used. The model predicts the grain orientation and ordering based on the spatial velocity gradient and particle shape ratio. The kinematic continuum model of grain orientation [18] and the isotropic granular $\mu(I)$ rheology has been adopted as the frameworks in this study.

By using the representation theorem for isotropic tensor-valued functions of a tensor variable, a full description of the new stress model that is a function of the grain orientation (\mathbf{A}), rate of deformation (\mathbf{D}), effective viscosity $\mu(I)$, shape ratio (r_g) and pressure has been obtained. A simpler model has been formed with the linear terms in \mathbf{A} with two material parameters, the functions of the shape ratio, from the full description of the isotropic function. The dissipation inequality has been used as a guide towards the restrictions on the material parameters. The material parameter ϕ is interpreted as it governs the interlocking behaviour of the elongated grains, and it must be greater than or equal to zero according to the dissipation inequality. On the other hand, the material parameter η is interpreted as it governs the ability of the grains to orient themselves with the streamlines of the flow. Dissipation inequality postulated that η must be greater than or equal to -1 in 3-D cases. The finalized 3-D model has been tested with the data extracted from [19]. The model was found to be capable to capture the non-monotonous behaviour that has been observed in the critical viscosity of the steady-state simple shear flow. The model predictions very well captured the stress response of the system. Some deviation between the model and the experimental data has been observed in the diagonal components of the Cauchy stress tensor when the shape ratio of the grains is higher than 0.2. However, even in the highest deficit case, the model predictions were only off by 9.7%.

To reveal the full capabilities of the proposed continuum model, a complete 2-D transient problem was selected to be solved. The simple shear flow has been selected due to its simplicity and experimental data availability. The 3-D model has been converted to the 2-D form by introducing another term from the isotropic representation theorem. A new term in the model required additional material parameters to be

included. In this case, since there are two independent variables that the Cauchy stress tensor offers, the new material parameter ν taken to be equal to the material parameter η . The finalized 2-D form of the constitutive model was tested with the experimental data obtained from [25]. The model was able to capture the shear stress response of the simple shear flow with less than $10^{-2}\%$ error. On the other hand, the components T_{11} and T_{22} were off by 22% and 20% respectively. This discrepancy did not raise concern since the experimental data extracted from a journal article in the literature, and a better fit could be achieved by altering the cost function that has been used for the optimization problem.

The mechanical response and the orientation of the grains throughout the flow have been studied with 3 different grains. The first type was the spherical grains with a shape ratio of 0. Spherical grains took the material parameters as $\phi = 1$ and $\eta = 0$, hence the model boiled down to the well-received $\mu(I)$ rheology. The shear stresses generated had no change in time for the spherical grains since they do not have the ability to self orient themselves along the streamlines of the flow. Due to the shape isotropy, the orientation of the spherical grains is always isotropic. Hence, no change in the shear stress generated in this case did not change in time. Grains with the shape ratio of 0.5 showed two strong players acting on the mechanical response of the system. The shear stress (T_{12}) showed a non-monotonic character as expected. It decreased as the grains started to align with the flow direction and increased after the A_{11} component surpassed 0.7 due to the interlocking behaviour of the elongated grains. On the other hand, grains with the shape ratio of 0.2 showed a similar but less strong character since they do not have a strong ability to self orient themselves with the flow streamlines and interlocking character. The steady-state shear stress predictions of the model agreed with the experimental work reported in [19,25]. The grains with the shape ratio of 0.5 were found to be easier to shear compared to spherical and grains with the shape ratio of 0.2. Also, despite the grains with the shape ratio of 0.2 have the ability to orient themselves in the shear direction, they are harder to shear compared to the spherical grains.

The orientation of the grains throughout the flow is analyzed with the components of the structure tensor \mathbf{A} . In other words, the second-moment matrix's components represent the predominant directions that the particles are pointing. A_{11} and A_{22} components of the structure tensor can be interpreted as they show the number of particles that are aligned in those axes. Since the more elongated particles have a stronger ability to self orient themselves with the flow streamlines, A_{11} component of

the grains with the shape ratio of 0.5 at the steady-state is higher compared to the grains with the shape ratio of 0.2. Furthermore, the change of A_{11} component over time revealed that the kinematic model predicted that the more elongated particles align with the streamlines faster compared to the less elongated particles. At this time, there is no available numerical or experimental work that supports or reports the same behaviour. A closer look at the A_{22} component showed the same characteristics with the A_{11} component. More elongated particles ($r_g = 0.5$) reached 0.15 where, on the other hand, less elongated particles ($r_g = 0.2$) reached 0.31 at the steady-state which indicates that fewer particles are aligned with the streamlines in the case of less elongated particles. The change of the component A_{12} of the structure tensor over time revealed that more particles are rotating, and they are faster to align with the shear direction when the elongation of the grain increases. The dissipation inequality has been calculated at every point in space at every instant of time to make sure it has not been violated throughout the deformation.

In a nutshell, the study succeeds its main objective of proposing a continuum stress response model that accounts for the grain shape and orientation. The proposed model's predictions agreed with the available numerical and experimental data, and it was able to capture the non-monotonic behaviour observed in the critical viscosity (μ_s). In the future, the model should be tested in 3-D problems. Most of the real-world applications of the shape anisotropic granular rheology deal with the grains in all 3 coordinates. This study is a step ahead showing the capabilities of the model in a 2-D case.

Appendix A

Additional Information

A.1 Governing Equations of the Reverse Direction

A.1.1 Linear Momentum Balance equations

$$0 = -\frac{\partial P}{\partial x_2} + \mu_s \phi \eta \left[\frac{\partial P}{\partial x_2} A_{22} + P \frac{\partial A_{22}}{\partial x_2} - \frac{\partial P}{\partial x_2} \frac{1}{2} \right] \quad (\text{A.1})$$

$$\begin{aligned} \rho \frac{\partial v}{\partial t} = & -\frac{\mu_s \phi}{\sqrt{2}} \frac{\partial P}{\partial x_2} - \frac{\mu_s \phi \eta}{\sqrt{2}} \left[\frac{\partial P}{\partial x_2} A_{22} + P \frac{\partial A_{22}}{\partial x_2} + \frac{\partial P}{\partial x_2} A_{11} + P \frac{\partial A_{11}}{\partial x_2} \right] \\ & + \mu_s \phi \eta \left[\frac{\partial P}{\partial x_2} A_{12} + P \frac{\partial A_{12}}{\partial x_2} \right] \quad (\text{A.2}) \end{aligned}$$

A.1.2 Equations from the Evolution of Structure Tensor

$$\frac{\partial A_{11}}{\partial t} = \frac{\partial v}{\partial x_2} \left[-A_{12} - \lambda A_{12} + 2\lambda A_{12} A_{11} - \frac{\psi}{\sqrt{2}} A_{11} + \frac{\psi}{2\sqrt{2}} \right] \quad (\text{A.3})$$

$$\frac{\partial A_{12}}{\partial t} = \frac{\partial v}{\partial x_2} \left[-\frac{A_{22}}{2} + \frac{A_{11}}{2} - \frac{\lambda}{2} (A_{11} + A_{22}) + 2\lambda A_{12}^2 - \frac{\psi A_{12}}{\sqrt{2}} \right] \quad (\text{A.4})$$

$$\frac{\partial A_{22}}{\partial t} = \frac{\partial v}{\partial x_2} \left[A_{12} - \lambda A_{12} + 2\lambda A_{12} A_{22} - \frac{\psi}{\sqrt{2}} A_{22} + \frac{\psi}{2\sqrt{2}} \right] \quad (\text{A.5})$$

Bibliography

- [1] Christophe Ancey, Philippe Coussot, and Pierre Evesque. A theoretical framework for granular suspensions in a steady simple shear flow. *Journal of Rheology*, 43(6):1673–1699, 1999.
- [2] Igor S Aranson and Lev S Tsimring. Continuum description of avalanches in granular media. *Physical Review E*, 64(2):020301, 2001.
- [3] Emilien Azéma, Itthichai Preechawuttipong, and Farhang Radjai. Binary mixtures of disks and elongated particles: Texture and mechanical properties. *Physical Review E*, 94(4):042901, 2016.
- [4] Emilien Azéma and Farhang Radjai. Stress-strain behavior and geometrical properties of packings of elongated particles. *Physical Review E*, 81(5):051304, 2010.
- [5] Tamás Börzsönyi, Balázs Szabó, Gábor Törös, Sandra Wegner, János Török, Ellák Somfai, Tomasz Bien, and Ralf Stannarius. Orientational order and alignment of elongated particles induced by shear. *Physical review letters*, 108(22):228302, 2012.
- [6] Julien Chauchat and Marc Médale. A three-dimensional numerical model for dense granular flows based on the μ (i) rheology. *Journal of Computational Physics*, 256:696–712, 2014.
- [7] Paul W Cleary and Mark L Sawley. Dem modelling of industrial granular flows: 3d case studies and the effect of particle shape on hopper discharge. *Applied Mathematical Modelling*, 26(2):89–111, 2002.
- [8] Frédéric Da Cruz, Sacha Emam, Michaël Prochnow, Jean-Noël Roux, and François Chevoir. Rheophysics of dense granular materials: Discrete simulation of plane shear flows. *Physical Review E*, 72(2):021309, 2005.

- [9] Gustavo Düring, Edan Lerner, and Matthieu Wyart. Effect of particle collisions in dense suspension flows. *Physical Review E*, 94(2):022601, 2016.
- [10] Somayeh Farhadi and Robert P Behringer. Dynamics of sheared ellipses and circular disks: effects of particle shape. *Physical review letters*, 112(14):148301, 2014.
- [11] Isaac Goldhirsch. Rapid granular flows. *Annual review of fluid mechanics*, 35(1):267–293, 2003.
- [12] Romain Guises, Jiansheng Xiang, John-Paul Latham, and Antonio Munjiza. Granular packing: numerical simulation and the characterisation of the effect of particle shape. *Granular Matter*, 11(5):281–292, 2009.
- [13] Raúl C Hidalgo, Balázs Szabó, Katalin Gillemot, Tamas Börzsönyi, and Thomas Weinhart. Rheological response of nonspherical granular flows down an incline. *Physical review fluids*, 3(7):074301, 2018.
- [14] Ivan Iordanoff and MM Khonsari. Granular lubrication: toward an understanding of the transition between kinetic and quasi-fluid regime. *J. Trib.*, 126(1):137–145, 2004.
- [15] Pierre Jop, Yoël Forterre, and Olivier Pouliquen. A constitutive law for dense granular flows. *Nature*, 441(7094):727, 2006.
- [16] Jun Katagiri, Takashi Matsushima, and Yasuo Yamada. Simple shear simulation of 3d irregularly-shaped particles by image-based dem. *Granular Matter*, 12(5):491–497, 2010.
- [17] P Mills, D Loggia, and M Tixier. Model for a stationary dense granular flow along an inclined wall. *EPL (Europhysics Letters)*, 45(6):733, 1999.
- [18] B Nadler, F Guillard, and I Einav. Kinematic model of transient shape-induced anisotropy in dense granular flow. *Physical review letters*, 120(19):198003, 2018.
- [19] Dániel B Nagy, Philippe Claudin, Tamás Börzsönyi, and Ellák Somfai. Rheology of dense granular flows for elongated particles. *Physical Review E*, 96(6):062903, 2017.

- [20] Dániel B Nagy, Philippe Claudin, Tamás Börzsönyi, and Ellák Somfai. Flow and rheology of frictional elongated grains. *New Journal of Physics*, 22(7):073008, 2020.
- [21] Ronald Midgley Nedderman. *Statics and kinematics of granular materials*. Cambridge University Press, 2005.
- [22] SB Savage. Analyses of slow high-concentration flows of granular materials. *Journal of Fluid Mechanics*, 377:1–26, 1998.
- [23] Stuart B Savage. The mechanics of rapid granular flows. In *Advances in applied mechanics*, volume 24, pages 289–366. Elsevier, 1984.
- [24] Ellák Somfai, Dániel B Nagy, Philippe Claudin, Adeline Favier, Dávid Kálmán, and Tamás Börzsönyi. Effective friction of granular flows made of non-spherical particles. In *EPJ Web of Conferences*, volume 140, page 03062. EDP Sciences, 2017.
- [25] Martin Trulsson. Rheology and shear jamming of frictional ellipses. *Journal of Fluid Mechanics*, 849:718–740, 2018.
- [26] CC Wang. On representations for isotropic functions. *Archive for rational mechanics and analysis*, 33(4):249–267, 1969.
- [27] Sandra Wegner, Ralf Stannarius, Axel Boese, Georg Rose, Balazs Szabo, Ellak Somfai, and Tamás Börzsönyi. Effects of grain shape on packing and dilatancy of sheared granular materials. *Soft Matter*, 10(28):5157–5167, 2014.
- [28] Yu Zhou, Huabin Wang, Bo Zhou, and Jianmei Li. Dem-aided direct shear testing of granular sands incorporating realistic particle shape. *Granular Matter*, 20(3):55, 2018.